We are IntechOpen, the world's leading publisher of Open Access books
Built by scientists, for scientists

6,900
Open access books available

186,000
International authors and editors

200M
Downloads

154
Countries delivered to

Our authors are among the

TOP 1%
most cited scientists

12.2%
Contributors from top 500 universities

CLARIVATE ANALYTICS
BOOK CITATION INDEX
INDEXED

WEB OF SCIENCE™

Selection of our books indexed in the Book Citation Index
in Web of Science™ Core Collection (BKCI)

Interested in publishing with us?
Contact book.department@intechopen.com

12

Optical MEMS

Wibool Piyawattanametha[1,2] and Zhen Qiu[3]
*[1]Advanced Imaging Research (AIR) Center, Faculty of Medicine,
Chulalongkorn University, Pathumwan,
[2]National Electronics and Computer Technology Center, Pathumthani,
[3]University of Michigan, Biomedical Engineering, Ann Arbor, Michigan
[1,2]Thailand
[3]USA*

1. Introduction

In 1989, a group of scientists and engineers in Salt Lake City started a workshop called Micro-Tele-Operated Robotics Workshop. There, the acronym for Microelectromechanical systems (MEMS) was officially adopted. However, MEMS technology has already had a head start since at least 7 years ago from the classic work published by Petersen in 1982 [1]. Twenty years later, MEMS technology has started major novel innovations in several scientific fields and created highly promising market potential. In 2003, the most conservative market studies predict a world MEMS market in excess of $8 billion.

Optics and photonics are among these research fields impacted by MEMS techniques. Optical MEMS has created a new fabrication paradigm for optical devices and systems. These micro optical devices and systems are inherently suited for cost effective wafer scale manufacturing as the processes are derived from the semiconductor industry. The ability to steer or direct light is one of the key requirements in optical MEMS. In the past two decades since Petersen published his silicon scanner [1], the field of optical MEMS has experienced explosive growth [2,3]. In the 80's and early 90's, displays were the main driving force for the development of micromirror arrays. Portable digital displays are commonplaces and head mount displays are now commercially available. In the past decade, telecommunications have become the market driver for Optical MEMS. The demand for routing internet traffic through fiber optic networks pushes the development of both digital and scanning micromirror systems for large port-count all-optical switches with the ability to directly manipulate an optical signal, Optical MEMS systems eliminate unnecessary optical-electrical-optical (O-E-O) conversions. In the biomedical arena, micro-optical scanners promise low-cost endoscopic three-dimensional imaging systems for *in vivo* diagnostics.

This chapter summarizes the state of the art of Optical MEMS technology by describing basic fabrication processes to derive with actuation mechanisms and select examples of devices that are either commercially available, or show great promise of becoming products in the near term. The chapter is organized into the following sections: Section 2 describes the generic actuation mechanisms commonly used for MEMS devices. Section 3 discusses the applications.

2. Mechanisms of actuations

Since the actuators are important engines for Optical MEMS, we will introduce different kinds of actuation mechanisms first and explain the working principles in detail. Furthermore, for more specific applications, there are many variants or requirements based on these basic actuation mechanisms.

2.1 Electrostatic actuation

Electrostatic MEMS devices work at different motion modes. Here we mainly introduce the MEMS devices with torsional rotation. Electrostatic MEMS devices with torsional rotation can be described as follows: when voltage is applied between the movable and the fixed electrodes, the moving part rotates about the torsion axis until the restoring torque and the electrostatic torque are equal. The torques can be expressed as:

$$T_e(\theta) = \frac{V^2}{2} \frac{\partial C}{\partial \theta} \tag{1}$$

$$T_r(\theta) = k\theta \tag{2}$$

where V is the applied voltage across the fixed and movable electrodes, C is the capacitance of the actuator, θ is the rotation angle, and k is the spring constant. The capacitance is determined by the area of the electrode overlap and the gap between the electrodes. For simple parallel plate geometry, the capacitance can be expressed by

$$C = \frac{\varepsilon_0 A}{g} \tag{3}$$

where ε_0 is the permittivity of free space, A is the area of electrode overlap, and g is the gap between fixed and moving electrodes.

There are two major types of electrostatic actuators. The first is based on parallel-plate capacitance, and the other is based on comb-drive capacitance. For the parallel-plate type devices (Figure 2-1), the area of the electrode overlap is essentially the area of the fixed electrode. The gap for the parallel-plate actuator is a function of the rotation angle and there is a tradeoff as the initial gap spacing needs to be large enough to accommodate the scan angle, but small enough for reasonable actuation voltage. The stable scan range is further limited by a pull-in phenomenon to 34-40% of the maximum mechanical scan angle [4,5].

Another type of actuator is based on the vertical combdrive. The vertical combdrive offers several advantages: (1) the structure and the actuator are decoupled; (2) the gap between the interdigitated fingers of the combdrive is typically quite small, on the order of a couple of microns [6,7]. Large rotation angle and low actuation voltage can be achieved simultaneously. In the combdrive, the gap is constant and the area of the electrode overlap is a function of the rotation angle. Typically, there are three approaches to realize the vertical combdrive actuators. The first and popular one is the staggered vertical combdrive actuators [46]. Figure 2-2 shows the schematic of a vertical combdrive actuator. The second type is the angular vertical combdrive actuators [8,58,59] (Figure 2-3). Both staggered and angular vertical combdrive actuators can work at either resonant tilting mode or quasi-static (or called DC tilting) mode. At quasi-static mode, the maximum rotation angle usually is limited because it is typically the point where the overlap area of electrodes reaches the
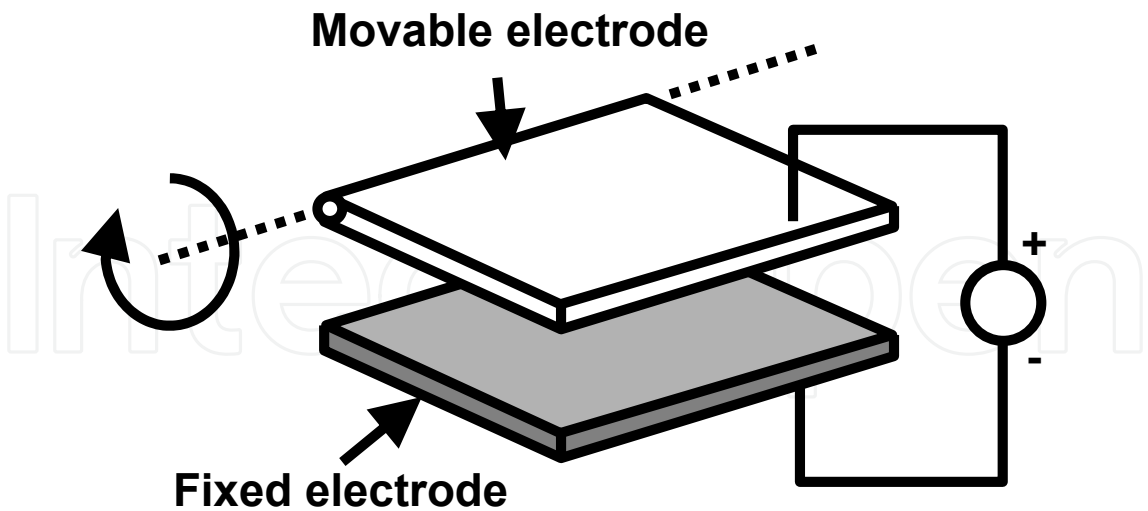
Fig. 2.1. Schematic of a parallel-plate actuator

maximum. In addition to the staggered and angular vertical combdrive actuators, in-plane configuration vertical combdrive actuator is the third approach firstly demonstrated by Harald [8] at Fraunhofer IPMS Dresden, Germany. The in-plane configuration vertical combdrive (Figure 2-4) means that the moving combdrive is on the same plane of the static combdrive, which is based on the parametric resonant working principle. The resonantly excited actuator has several advantages as below: (1) it can achieve very large tilting angle with low driving voltage; (2) only one-time DRIE is needed for combdrive and gimbal frame structure during micro-machining which eliminates wafer bonding or accurate alignment. However, the vertical combdrive actuators with in-plane configuration only work at resonant mode. Recently, researchers at IPMS also have made effort to realize quasi-static rotation mode with vertical out-of-plane combdrive using leverage structures [9].
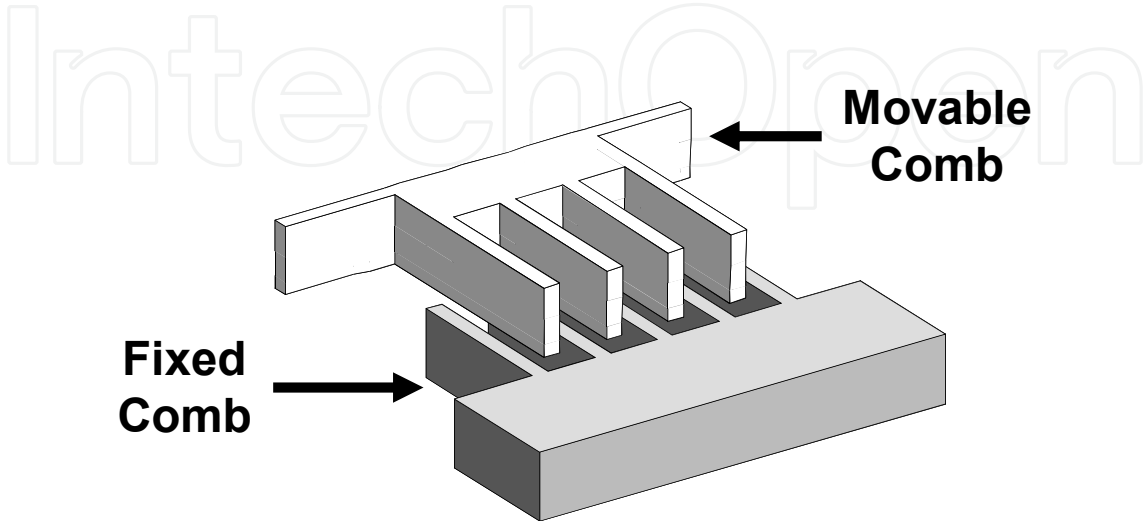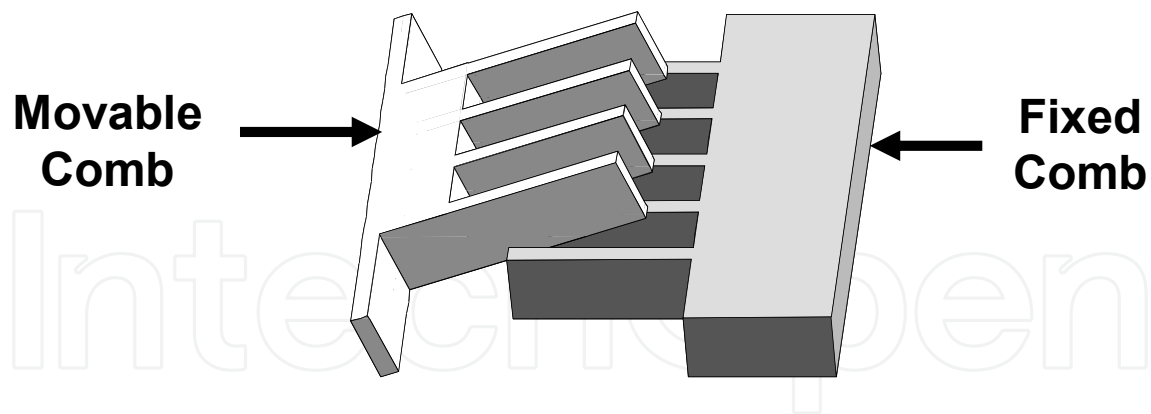

Fig. 2.2. Schematic of a vertical combdrive actuator
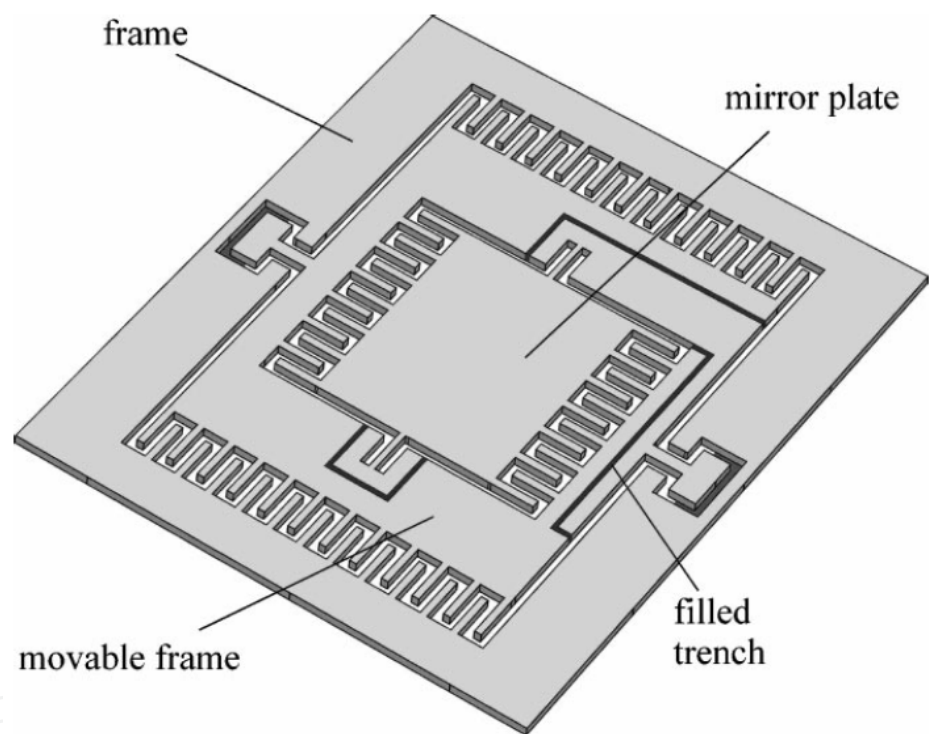
Fig. 2.3. Schematic of an angular combdrive actuator

Fig. 2.4. Schematic of an in-plane configuration combdrive actuator

2.2 Magnetic actuation

Magnetic actuation is practical when the structural dimensions are on the millimeter scale since the magnetic torque (generated by the magnetic device interacting with an external magnetic field) scales with volume for permanent magnetic materials and with total coil area for electromagnets. For an analysis of magnetic torque see Judy and Muller [10]. The overall system size must accommodate the magnets (permanent or electric coils) used to generate the external magnetic field. Therefore, the motivations for this type of scanner are usually cost reduction through batch fabrication and lower power consumption rather than miniaturization. In addition, magnetic actuation also has the advantage of operating in liquid environment.

Magnetic field can be induced by electrical current. This current-induced magnetic field can generate the force exerted on the moving magnetic material [10]. While the moving structure is not made of magnetic material, electromagnetic coils can be integrated on the movable part, making it quasi-magnetic by current injection [11]. Figure 2-5 shows an example of the electromagnetic scanner that is being used in table-top confocal microscopes. Researchers at the University of Michigan have demonstrated a miniature magnetic 3D scanner for optical alignment [12] shown in Figure 2-6.
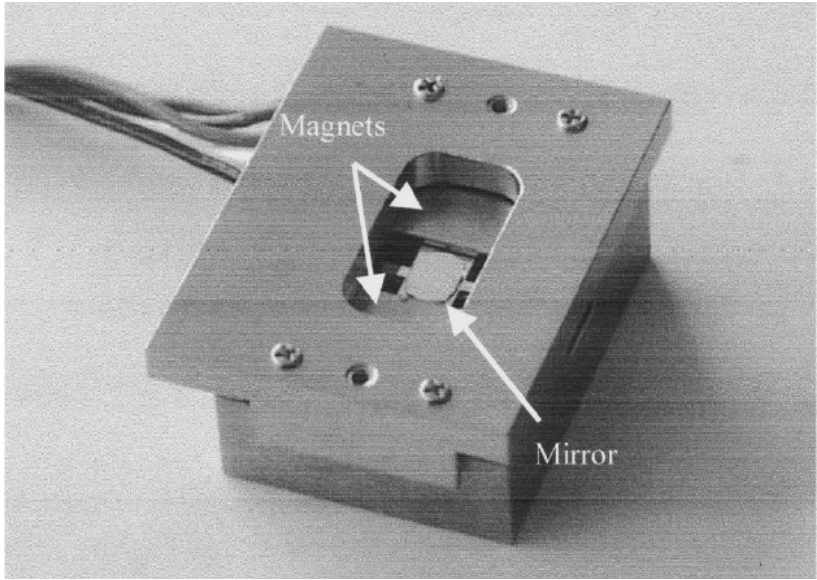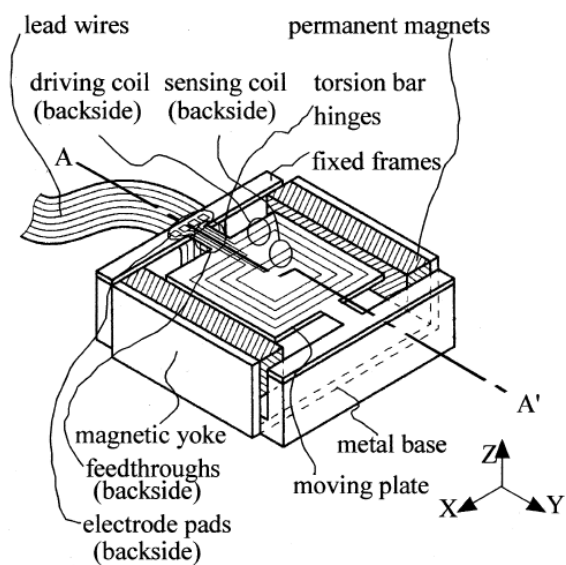
Fig. 2.5. (a) Schematic and (b) photograph of packaged electromagnetic 1D scanner in [11] (Picture courtesy of Hiroshi Miyajima).
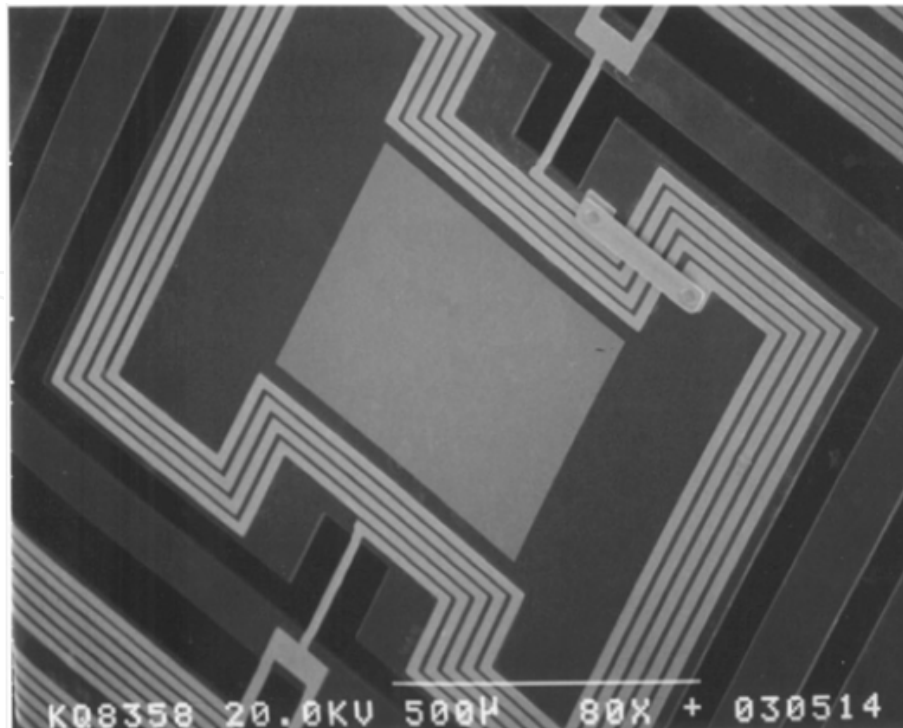
Fig. 2.6. SEM of the miniature electromagnetic 3D scanner in [12]
(Picture courtesy of Il-Joo Cho).

2.3 Thermal actuation

Thermal actuation utilizes the mismatch between thermal expansion coefficients of materials, which yields structural stress after temperature change. The structure deforms due to this built-in stress. The major advantage of thermal actuation is its ability to generate large deflection. Electrical current injection is one of the common mechanisms used for heating up the structure. However, temperature control and power consumption are issues for this type of actuators. Several new electro-thermal micromirror and actuators have been reported [13,14,15,16,17,18] by researchers from University of Florida. For example, shown in Figure 2-7, the electrothermal bimorph structure in [17] is based on two thin-film materials with different coefficients of thermal expansion(CTE), like Aluminum (high CTE) and SiO2 (low CTE). The heater material can be polysilicon or Pt. The induced thermal bending arc angle (θ_T) of the bimorph beam can be expressed as below

$$\theta_T = \theta_0 - \theta_1 = \beta \cdot \frac{l_b}{t_b} \cdot \Delta\alpha \cdot \overline{\Delta T}$$

Where θ_0 and θ_1 are the arc angles before and after the temperature increase, t_b and l_b are the bimorph thickness and length, $\Delta\alpha$ is the CTE difference of the two bimorph materials, β is the actuation coefficient related to the thickness and biaxial Young's Modulus ratios of the two materials, and $\overline{\Delta T}$ is the average temperature change on the bimorph.

The electrothermal microactuator in [16], shown in Figure 2-8, using three-bimorph actuation mechanism can achieve large lateral-shift-free (LSF) piston motion at low driving voltage (5.3V) with thermal response time around 25ms. The design is potentially suitable

for both pure z-axis displacement actuator and large angle tilting mirror at low speed application.
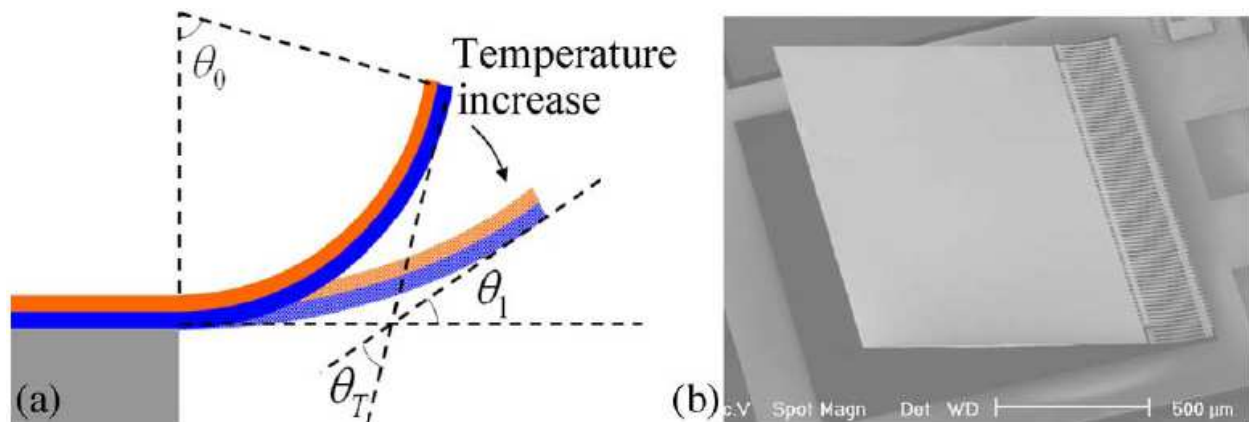

Fig. 2.7. Schematic show actuation principle of (a) a single bimorph and (b) SEM of a bimorph-based micromirror [17] (Picture courtesy of Huikai Xie).
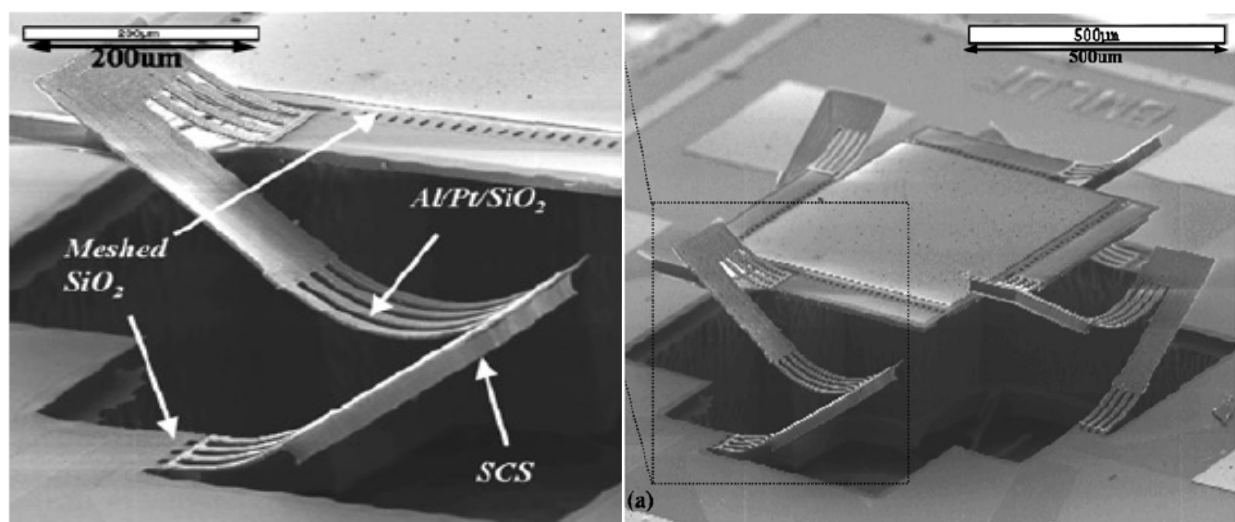

Fig. 2.8. Electrothermal bimorph microactuator with initial elevation in [16] (Picture courtesy of Huikai Xie)

2.4 Piezoelectric actuation mechanisms

Piezoelectric material deforms when electric field is applied across the structure. This property can be used as the driving mechanism in MEMS and NEMS. Different kinds of piezoelectric scanners and actuators have been demonstrated [19,20,21,22]. Using piezoelectric thin films, researchers at the University of Michigan have developed a novel thin-film lead zirconate titanate (PZT) based large displacement (around 120um) vertical translational microactuator [19]. The microactuator consists of four compound bend-up/bend-down unimorphs to generate z-axis motion of a moving stage. Figure 2-9 and Figure 2-10 show an example of the thin-film PZT based microactuator with large displacement. The large displacement within small footprint and high bandwidth (fast response) of the actuators at low-voltage and low-power levels should make them useful to a variety of optical applications, like endoscopic microscopy.
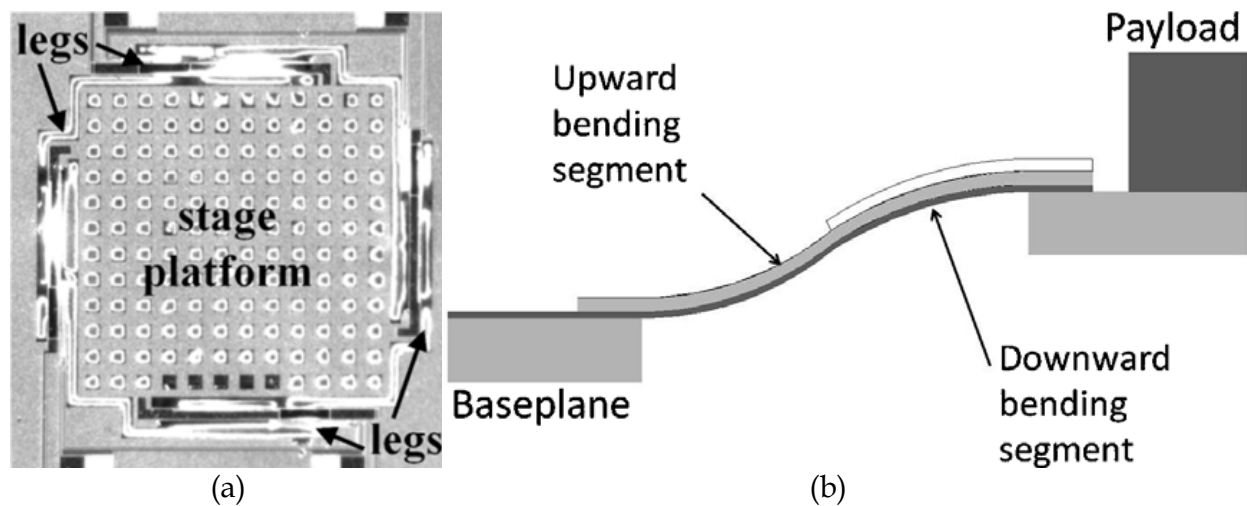
Fig. 2.9. (a) Top-view, piezoelectrically actuated vertical stage, (b) Schematic cross-section of a vertical translational stage in [19] (Picture courtesy of Kenn Oldham).
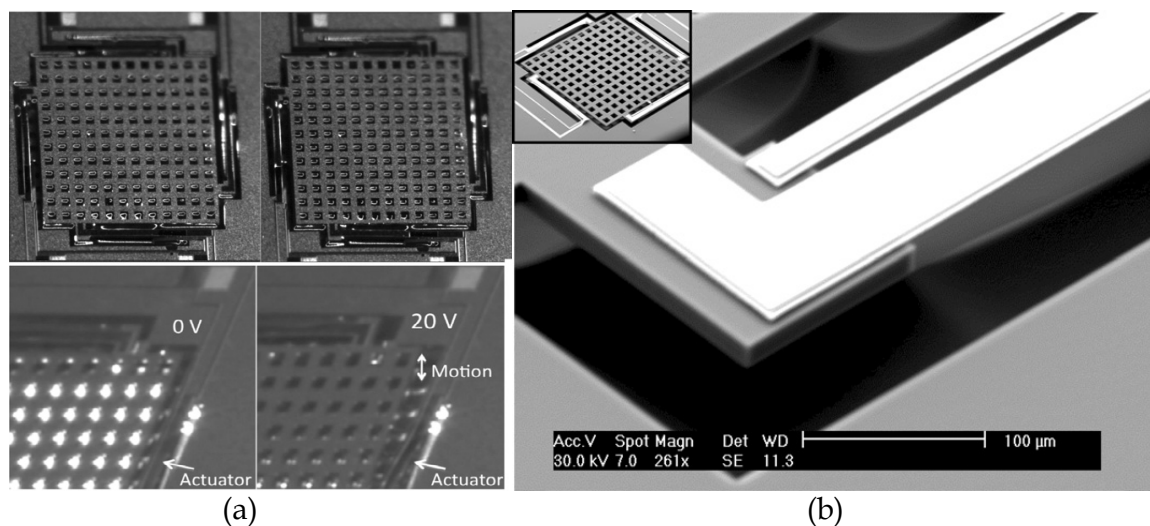

Fig. 2.10. (a) Top view and oblique view of the corner of a prototype vertical actuator under 0 and 20 V. (b) Scanning-electron microscope (SEM) image of end of an actuation leg (full actuator inset), showing the XeF2 etching profile below the device layer

Aluminium nitride (AlN) is another promising potential piezoelectric material for future Optical MEMS applications [21,22]. One of the important advantages of AlN is that it is very suitable for full CMOS compatible MEMS processes. Currently, researchers from IPMS Germany are developing quasistatic deformable mirrors by actively coupling lateral strain in micro machined AlN based membranes.

2.5 Other actuation mechanisms

Magnetostrictive materials transduce or convert magnetic energy to mechanical energy and vice versa. As a magnetostrictive material is magnetized, it strains; i.e., it exhibits a change in length per unit length. Conversely, if an external force produces a strain in a magnetostrictive material, the material's magnetic state will change. This bidirectional coupling between the magnetic and mechanical states of a magnetostrictive material

provides a transduction capability that is used for both actuation and sensing devices. It has the advantage of remote actuation by magnetic fields. 2D optical scanners using magnetostrictive actuators have been reported [23].

3. Applications

3.1 Display, imaging, and microscopy
3.1.1 Texas Instruments' Digital Micromirror Device (DMD)

The Digital Micromirror Device (DMD) started in 1977 by Texas Instruments. The DMD technology has helped revolutionize projector systems by dramatically decreasing costs and increasing performance from traditional projector systems which are based on LCD technology. The research initially focused on deformable mirror device. Eventually DMD becomes the preferred device. TI uses Digital Light Processing™ (DLP) to denote optical projection displays enabled by the DMD technologies [24].

The DMD is a reflective spatial light modulator (SLM) which consists of millions of digitally actuated micromirrors. Each micromirror is controlled by underlying complementary metal-oxide-semiconductor (CMOS) electronics, as shown in Figure 3-1. A DMD panel's micromirrors are mounted on tiny hinges that enable them to tilt either toward the light source (ON) or away from it (OFF) depending on the state of the static random access memory (SRAM) cell below each micromirror. The SRAM voltage is applied to the address electrodes, creating an electrostatic attraction to rotate the mirror to one side or the other. The details of operating principle, design, fabrication, and testing of DMD have been discussed in [25] and will not be repeated here.
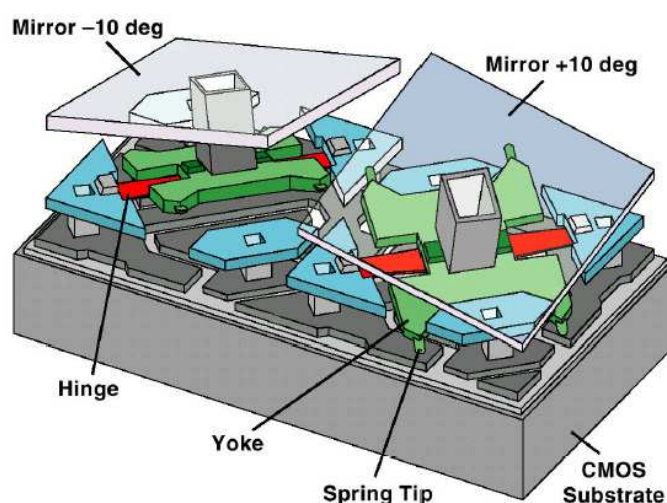

Fig. 3.1. Schematic drawing of two DMD mirror with underlying structures (Picture courtesy of TI. Reprinted from [24] with permission).

In projection systems, brightness and contrast are the two primary attributes that impact the quality of the projected image. The DMD has a light modulator efficiency in the range of 65%, and enables the contrast ratio ranging from 1000:1 to 2000:1. Because of the fast switching speed of the mirror, it enables the DLP to have a wide range of applications in video and data projectors, HDTVs, and digital cinema. Though, DMD was developed

primarily for projection display applications, there are some interesting non-display applications. An emerging new DMD application is volumetric display, in which DMDs are used to render three-dimensional images that appear to float in space without the use of encumbering stereo glasses or headsets. It is realized by using 3 DMD's to create 3D images viewed without glasses or headsets [26,27]. DMD also has applications in maskless lithography and telecom. Traditionally, the patterns in lithographic applications, such as print settings, printed circuit board (PCB) and semiconductor manufacturing, have been provided via film or photomasks. However, it is desirable to directly write on the UV-sensitive photoresist directly from digital files. DMD can be used as the spatial light modulator to generate the designed patterns [28]. For maskless lithography in sub-100nm semiconductor manufacturing, analog micromirror arrays with either tilting or piston motions are needed. Smaller mirror size is also desired.

DMD also has interesting applications in microscopy and spectroscopy. In microscopy application, DMD is used as a spatial modulator of the incident or collected light rays. It replaces the aperture in conventional optical system. The DMD can shape or scan either the illumination or collection aperture of an optical microscope thus to provide a dynamic optical system that can switch between bright field, dark field and confocal microscopy [29,30,31,32]. In spectroscopy application, the DMD is used as an adaptive slit selectively routing the wavelength of interest to a detector. It can also chop the light reaching the detector to improve detection sensitivity [33].

3.1.2 GLV display

The schematic of the Grating Light Valve™ (GLV™) shown in Figure 3-2 is a diffractive spatial light modulator [34]. The GLV device switches and modulates light intensities via diffraction rather than by reflection. Distinct advantages of GLV include high speed modulation, fine gray-scale attenuation, and scalability to small pixel dimensions.
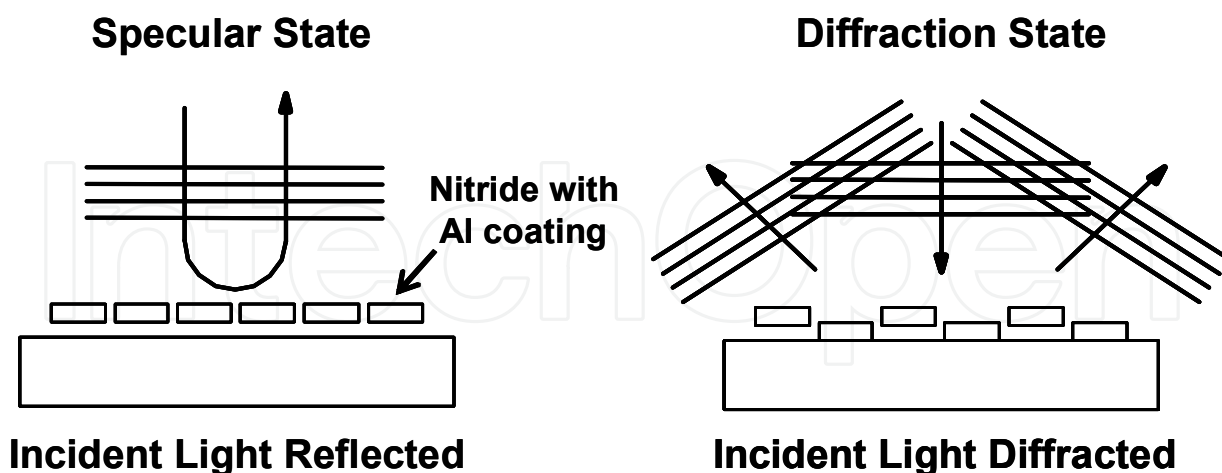

Fig. 3.2. Cross-section of the GLV device showing the specular and diffraction states
(after [34]).

The GLV device is built on a silicon wafer and is comprised of many parallel micro-ribbons that are suspended over an air gap above the substrate. Alternative rows of ribbons can be pulled down approximately ¼ wavelength to create diffraction effects on incident light by

applying an electrical bias between the ribbons and the substrate. When all the ribbons are in the same plane, the GLV device acts like a mirror and incident light is reflected from their surfaces. When alternate ribbons are deflected, the angular direction in which incident light is steered from the GLV device is dictated by the spatial frequency of the diffraction grating formed by the ribbons. As this spatial frequency is determined by the photolithographic mask used to form the GLV device in the fabrication process, the departure angles can be very accurately controlled, which is useful for optical switching applications. The linear deflection of the GLV is quite small, with no physical contact between moving elements, thus avoiding wear and tear as well as stiction problems. There are also no physical boundaries between the pixel elements in the GLV array. When using as a spatial light modulator in imaging applications, this seamless characteristic provides a virtual 100% fill-factor in the image.

The ribbons are made of suspended silicon nitride films with aluminum coating to increase its reflectivity. The silicon nitride film is under tensile stress to make them optically flat. The tension also reduces the risk of stiction and increases their frequency response. The GLV materials are compatible with standard CMOS foundry processes. GLV can be made into one-dimensional or two-dimensional arrays for projection display applications. Today, the GLV technology is used in high resolution display, digital imaging systems and WDM telecommunications [34].

3.1.3 Microvision retinal display and pico-projector

Retinal scanning display (RSD) uses a different approach from other microdisplays. Rather than a matrix array of individual modulator or source for each pixel as seen in liquid crystal display (LCD), organic light-emitting diodes (OLED), and DMD microdisplays, a RSD optimizes a low power light source to create a single pixel and scans this pixel with a single mirror to paint the displayed image directly onto the viewers' retina. With this technique, it offers high spatial and color resolution and very high luminance. There are several papers that provide an overview of the RSD and its applications [35,36]. This technology is developed by Microvision. The RSD systems typically employ two uniaxial scanners or one biaxial scanner. The combinations of two actuation mechanisms, electrostatic (for faster response) and electromagnetic (for larger force) actuations, were selected for a MEMS scanner [37]. Figure 3-3 shows a schematic drawing of the MEMS scanner.

The horizontal scanner (the inner mirror axis) is operated at resonance by using electrostatic actuation. The drive plates are located on the substrate below the MEMS mirror. The inner mirror axis has the resonant frequency of 19.5 kHz with the maximum mechanical scan excursion of 13.4 degrees. The vertical scanner (the outer mirror axis) is magnetically driven by means of permanent magnets within the package and cols with a 60 Hz linear ramp waveform. The magnets need to be positioned carefully and provide sufficient magnetic field to move the mirror to the desired angular deflection. The maximum mechanical scan excursion of 9.6 degrees was achieved on the outer mirror axis. The devices were bulk micromachined utilizing both wet and dry anisotropic etching and electroplating was used to form electromagnetic coils on the outer frame. These scanners must be stiff to remain flat and withstand the forces developed in resonant scanning mode. The dynamic mirror flatness of 0.05 microns rms was measured. The scanners also incorporate piezoresistive strain sensors on the torsion flexures for closed loop control. The scanners are designed to meet SVGA video standards that require 800 x 600 resolution. The design, fabrication, and control details of this bi-axial scanner can be found in [37] and [38].
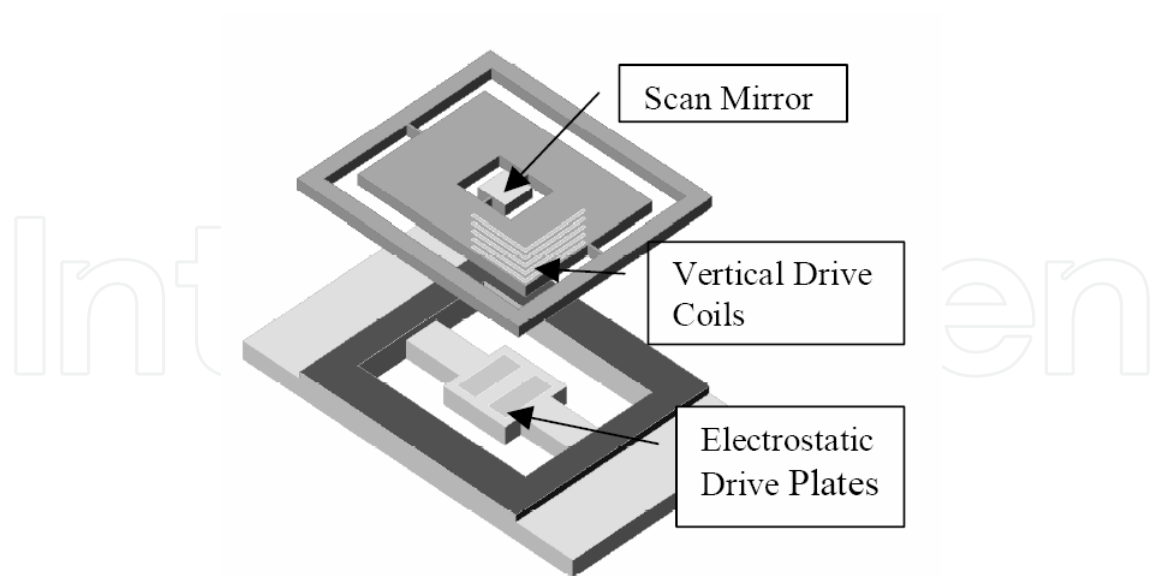
Fig. 3.3. Schematic drawing of the electrostatic/electromagnetic scanner
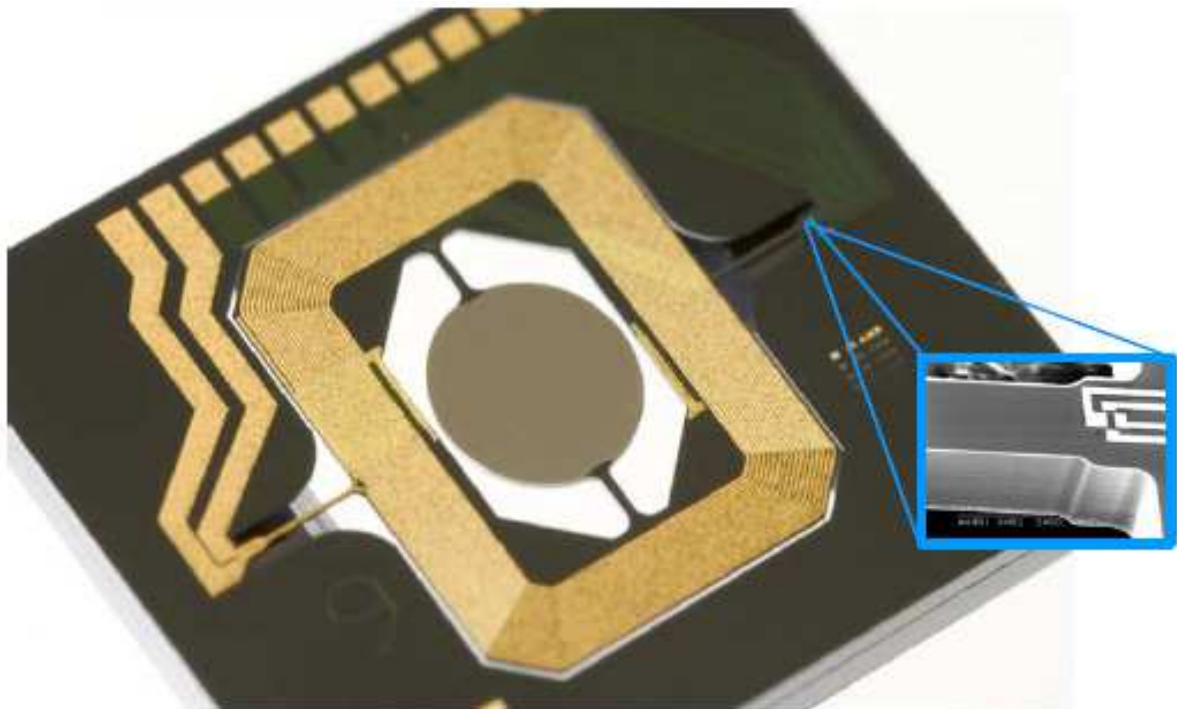(Picture courtesy of H. Urey. Reprinted from [37] with permission).

Fig. 3.4. MEMS scanning mirror die and close up of PZR strain sensor used for vertical scan
position feedback. (Picture courtesy of Davis, W.O.. Reprinted from [39] with permission).

A MEMS scanner based pico-projector system has been commercialized by Microvision [39].
Figure 3-4 shows a real magnetic dual-axis scanner die with piezo-resistor(PZR) strain
sensor for 2D raster scanning engine system.

3.1.4 Confocal microscopy and OCT (Optical Coherence Tomography)

Confocal microscopy offers several advantages over conventional optical microscopy, including controllable depth of field, the elimination of image degrading out-of-focus information, and the ability to collect serial optical sections from thick specimens. The concept was introduced by Marvin Minsky in the 1950's when he was a postdoctoral fellow at Harvard University. In 1957, he patented his "double-focusing stage-scanning microscope" in 1957 [40] which is the basis for the confocal microscope.

In a conventional widefield microscope, the entire specimen is bathed in light from a mercury or xenon source, and the image can be viewed directly by eye or projected onto an image capture device or photographic film. In contrast, the method of image formation in a confocal microscope is fundamentally different. Figure 3-5 shows the schematic drawing of the confocal imaging system. Illumination is achieved by scanning one or more focused beams of light, usually from a laser or arc-discharge source, across the specimen. This point of illumination is brought to focus in the specimen by the objective lens, and laterally scanned using some form of scanning device under computer control. The sequences of points of light from the specimen are detected by a photomultiplier tube (PMT) through a pinhole (or in some cases, a slit), and the output from the PMT is built into an image and displayed by the computer.

The scanning confocal optical microscope has been recognized for its unique ability to create clear images within thick, light scattering objects. This capability allows the confocal microscope to make high resolution images of living, intact tissues and has led to the expectation that confocal microscopy has become a useful tool for in vivo imaging.
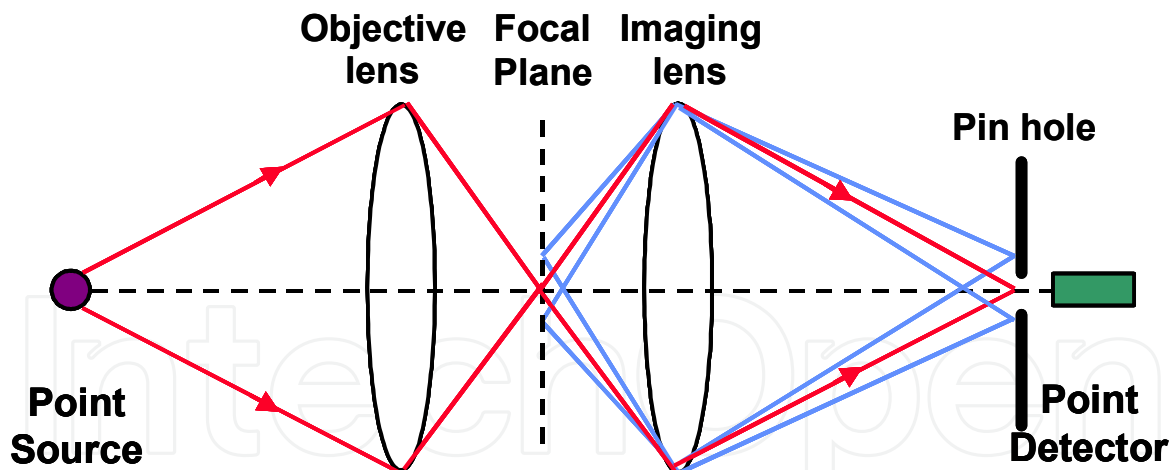

Fig. 3.5. Schematic drawing shows the concept of the confocal imaging system.

The first compact rectangle shape endoscope (2.5 mm (w) x 6.5 mm (l) x 1.2 mm (t)) based on MEMS scanning mirrors was developed by D.L. Dickensheets, et al. [41]. The architecture of the micromachined confocal optical scanning microscope, illustrated in Figure 3-6, consists of a single-mode optical fiber for illumination and detection, two cascaded one-dimensional bulk micromachined electrostatic scanners with orthogonal axes of rotation to accomplish x–y scanning, and a binary transmission grating as the objective lens. The maximum mechanical scanned angle is ±2 degrees. The resonant frequencies of both axes are over 1 kHz.
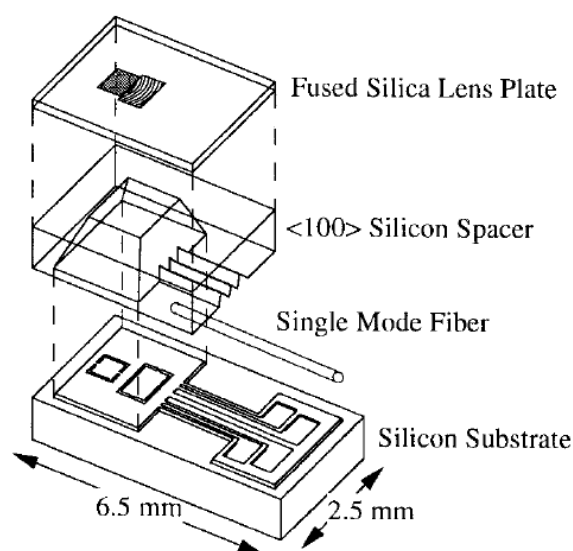
Fig. 3.6. Schematic drawing of the endoscope head showing various components of the assembly (Picture courtesy of D.L. Dickensheets. Reprinted from [41] with permission).

Later, Olympus Optical Company, Ltd. developed the first commercialized cylindrical shape confocal endoscope with an outside diameter of 3.3 mm and a length of 8 mm [42]. Figure 3-7 shows a cross sectional drawing of the endoscope head. The scanner is a gimbal based two-dimensional bulk micromachined electrostatic scanner [43] with the size of 1.3 mm x 1.3 mm. The mirror has the diameter of 500 um and resonant frequency of 3 kHz. The maximum mechanical scanned angle is ±3 degrees.
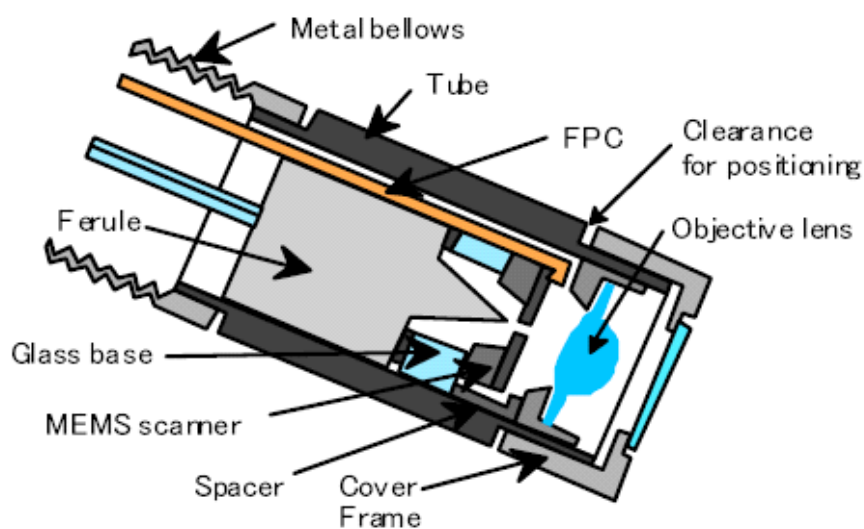

Fig. 3.7. A cross sectional drawing of the endoscope head (Picture courtesy of Olympus Optical Company, Ltd. Reprinted from [42] with permission).

Recently, researchers developed the dual-axis confocal (DAC) configuration,in Figure 3-8, to overcome conventional confocal microscope's limitations for endoscope compatibility and in vivo imaging by utilizing two optical fibers oriented along the intersecting optical axes of
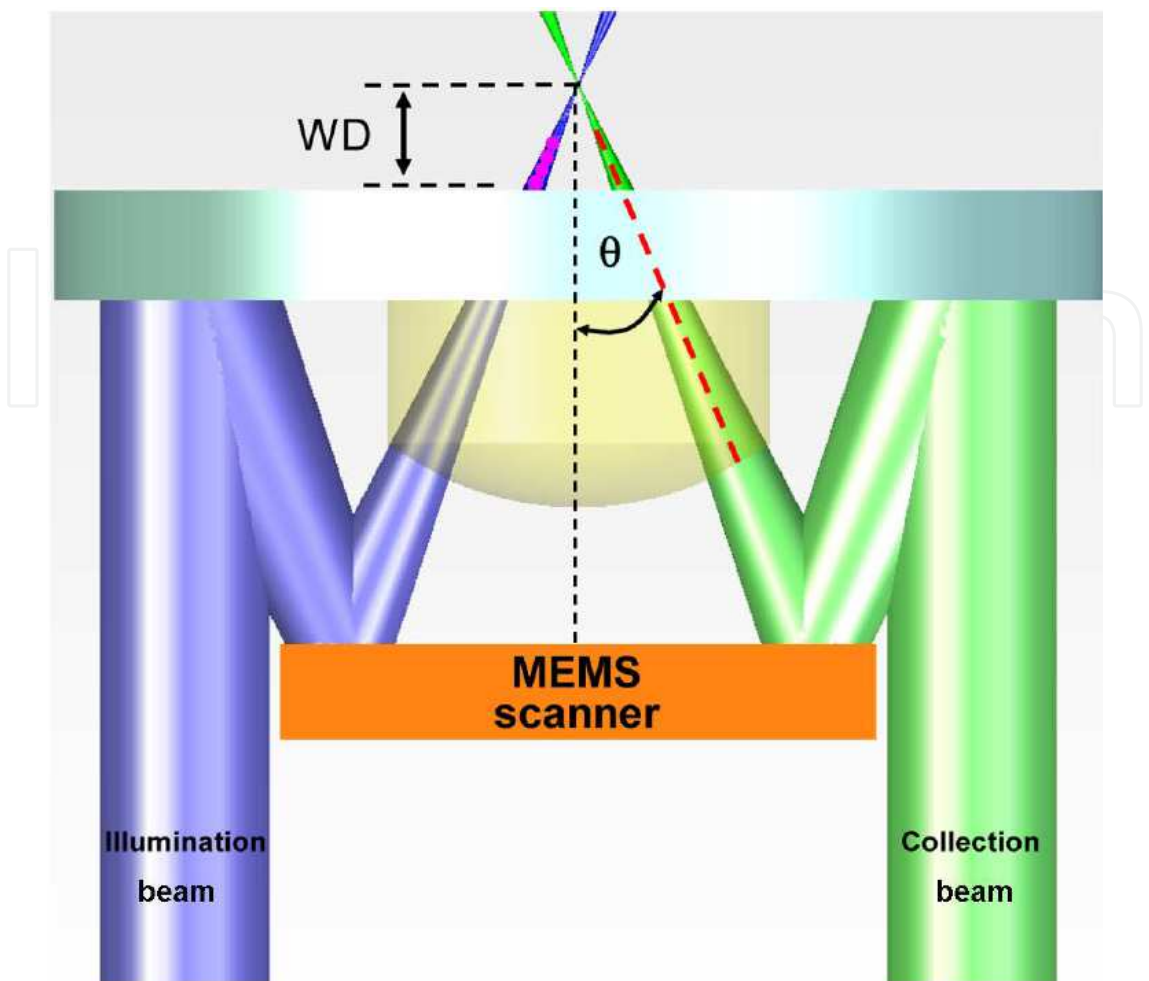
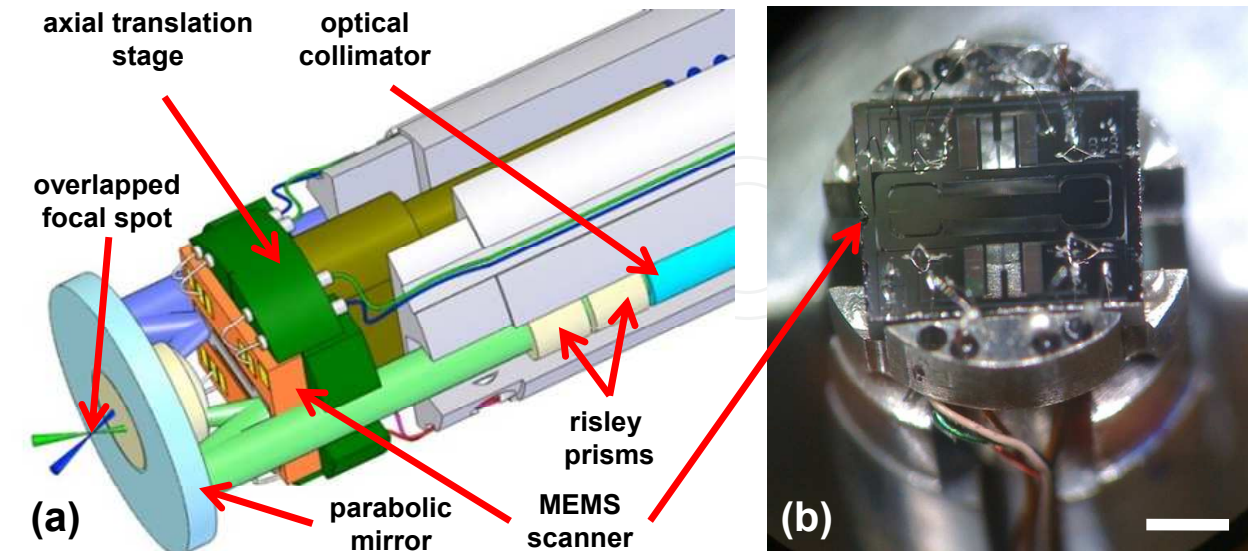Fig. 3.8. DAC microscope architecture (Reprinted from [49] with permission).

Fig. 3.9. A 5.5-mm diameter DAC microendoscope scanhead. (a) Two collimated beams are focused by a parabolic mirror. Real-time en face scanning is performed by a 2D MEMS scanner. (b) A photograph of the microendoscope without its cap shows a 2D MEMS scanner mounted on the axial translation stage, scale bar 3mm (Reprinted from [49] with permission).

two low-NA objectives to spatially separate the light paths for illumination and collection [44,45,46,47,48]. A state-of-the-art miniature (OD 5mm) 2D MEMS scanner based near-infrared dual-axis confocal microscopy system with z-axis focusing has been demonstrated, using 2D MEMS scanner. Figure 3-9 shows the schematic drawing of the whole system. It is the first time that MEMS device based endoscopy system, shown in Figure 3-10, has been used for in vivo imaging in human patients [49].
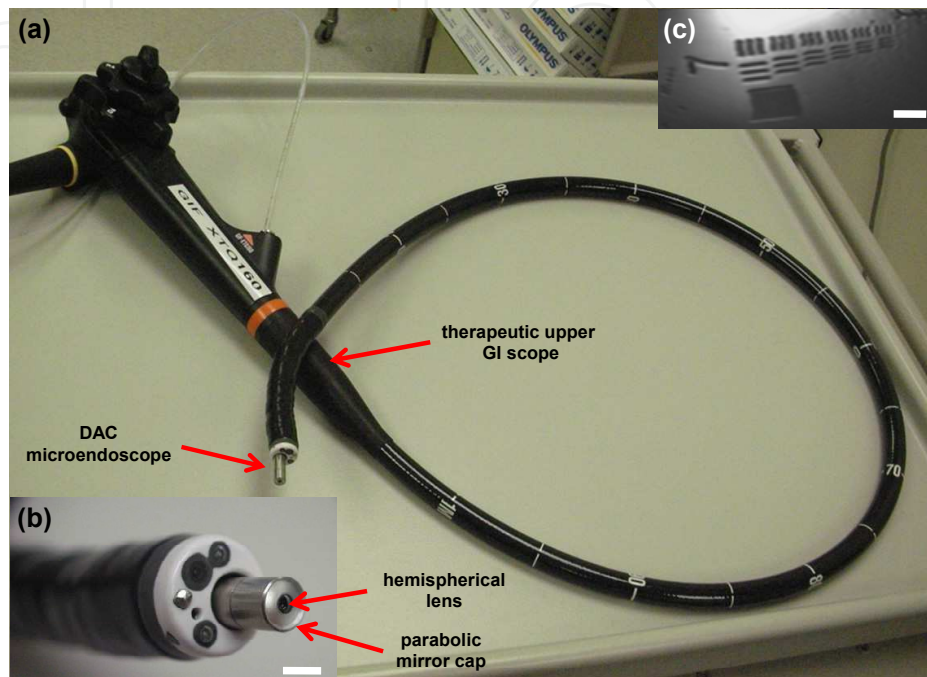

Fig. 3.10. (a) A DAC microendoscope is passed through the instrument channel of an Olympus XT-160 therapeutic endoscope that has a 6-mm diameter instrument channel. (b) Distal end of an endoscope shows the protruding DAC microendoscope, scale bar 5 mm. (c) Cropped reflectance image of a 1951 United States Air Force resolution test chart collected with the DAC microendoscope shows a transverse resolution of 5 μm, scale bar 20 μm (Reprinted from [49] with permission).

Optical coherence tomography (OCT) is an optical imaging technique that is analogous to B-mode medical ultrasound except that it uses low coherent light (low coherence interferometry) instead of sound. Generally, OCT imaging is performed using a fiber-optic Michelson interferometer with a low-coherence-length light source. Figure 3-11 shows the schematic drawing of the Michelson-type interferometer. One interferometer arm contains a modular probe that focuses and scans the light onto the sample, also collecting the backscattered light. The second interferometer arm is a reference path with a translating mirror or scanning delay line. Optical interference between the light from the sample and reference paths occurs only when the distance traveled by the light in both paths matches to within the coherence length of the light [50]. The interference fringes are detected and demodulated to produce a measurement of the magnitude and echo delay time of light backscattered from structures inside the tissue. The obtained data constitute a two-dimensional map of the backscattering or back reflection from internal architectural morphology and cellular structures in the tissue. Image formation is obtained by perform repeated axial measurement at different transverse positions as the optical beam is scanned across the tissue.
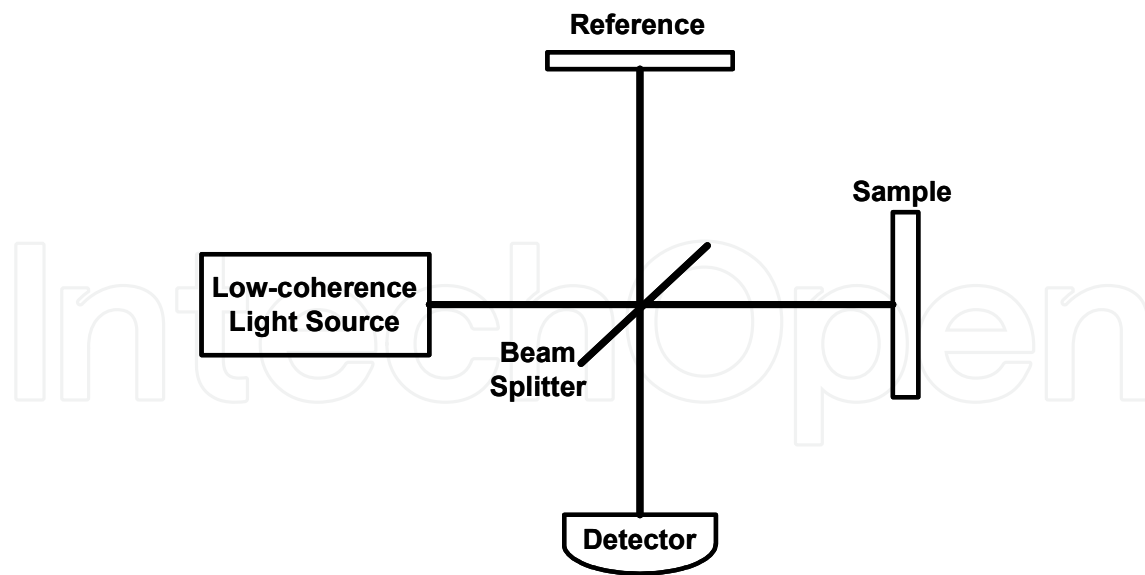
Fig. 3.11. Schematic drawing of a Michelson-type interferometer.

Since its initial use for imaging the transparent and low-scattering tissue of eyes [51], OCT has become attractive for noninvasive medical imaging. Real time in vivo endoscope based OCT imaging systems [52] of the gastrointestinal and respiratory tracts of a rabbit were demonstrated with an axial resolution of 10 um and sensitivity of more than 100 dB. The catheter-endoscope consisted of an encased, rotating hollow cable carrying a single-mode optical fiber.

Previously, the scanning element inside the OCT probe head used in clinical trials uses a spinning reflective element to scan the light beam across the tissue in circumferential scan geometry [52, 53]. This scanning arrangement allows the imaging probe to view only targets that are directly adjacent to the probe. The scan control of the probe is located outside the probe (proximal actuation). This type of actuation has some drawbacks such as a non-uniform and slow speed scanning. In addition, by applying a rotating torque on the optical fiber, it can cause unwanted polarization effects that can degrade image quality.

By using MEMS scanning mirrors, the scan control is located inside the probe head (distal actuation) which can reduce the complexity of scan control and potentially have a lower cost. Because of the scanner's miniature size, the overall diameter of the endoscope can be very small (< 5 mm). High speed and large transverse scan can also be achieved which enables real time in vivo imaging and large field of view, respectively.

Therefore, a need for compact, robust, and low cost scanning devices for endoscopic applications has fueled the development of MEMS scanning mirrors for OCT applications. Y. Pan, et al. developed a one-axis electro-thermal CMOS MEMS scanner for endoscopic OCT [54]. The mirror size is 1 mm by 1 mm. The SEM is shown in Figure 3-12. The bimorph beams are composed of a 0.7-um-thick Al layer coated on top of a 1.2-um-thick SiO_2 layer embedded with a 0.2-um-thick poly-Si layer. The mirror is coated with a 0.7-um-thick Al layer, and the underlying 40-um-thick single-crystal Si makes the mirror flat. The maximum optical scanned angle is 37 degrees (only in one direction).

Later, J.M. Zara, et. al fabricated one dimensional bulk micromachined MEMS scanner [55]. The scanner (1.5 mm long) is a gold-plated silicon mirror bonded on a 30-um-thick flat polyimide surface (2 mm long and 2.5 mm wide) that pivots on 3-um-thick polyimide

torsion hinges. Figure 3-13 shows an optical image of the endoscope head. The actuator used to tilt the mirror, the integrated force array (IFA), is a network of hundreds of thousands of micrometer-scale deformable capacitors. The capacitive cells contract because of the presence of electrostatic forces produced by a differential voltage applied across the capacitor electrodes.
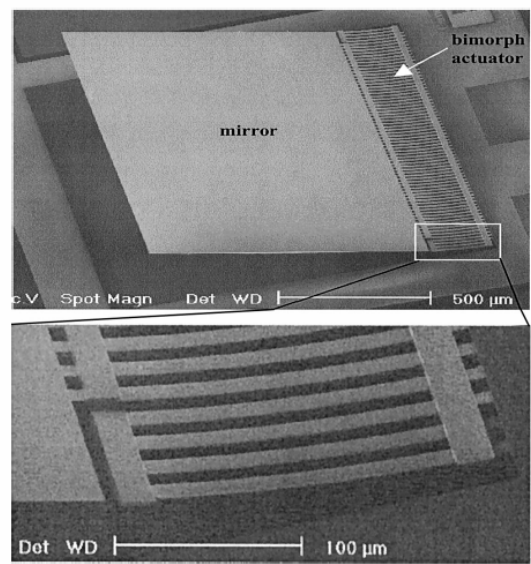

Fig. 3.12. SEM of electro-thermal CMOS MEMS scanner with an inset shows a close-up view of the bending springs (Picture courtesy of T. Xie. Reprinted from [54] with permission).
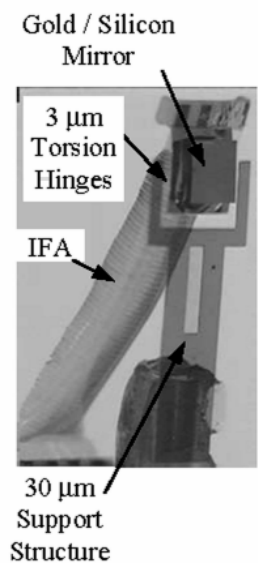

Fig. 3.13. An optical image of the endoscope head (Picture courtesy of J.M. Zara. Reprinted from [55] with permission).

Researchers at MIT and UCLA [56] have developed the first two-dimensional endoscopic MEMS scanner for high resolution optical coherence tomography. The two dimensional scanner with angular vertical comb actuators (AVC) is fabricated by using surface and bulk

micromachining techniques [57]. The angular vertical comb (AVC) bank actuators provide high-angle scanning at low applied voltage [58]. The combination of both fabrication techniques enables high actuation force, large flat micromirrors, flexible electrical interconnect, and tightly-controlled spring constants [58,59]. The schematic drawing of the 2D scanner is illustrated in Figure 3-14. An single-crystalline silicon (SCS) micromirror is suspended inside a gimbal frame by a pair of polysilicon torsion springs. The gimbal frame is supported by two pairs of polysilicon torsion springs. The four electrically isolated torsion beams also provide three independent voltages (V_1 to V_3) to inner gimbals and mirrors. The torsion spring is 345 μm long, 10 or 12 μm wide, and 3.5 μm thick. The scanner has 8 comb banks with 10 movable fingers each. The finger is 4.6 μm wide, 242 μm long, and 35 μm thick. The gap spacing between comb fingers is 4.4 μm. The mirror is 1000 μm in diameter and 35 μm thick. The AVC banks are fabricated on SCS. The movable and fixed comb banks are completely self-aligned [58].
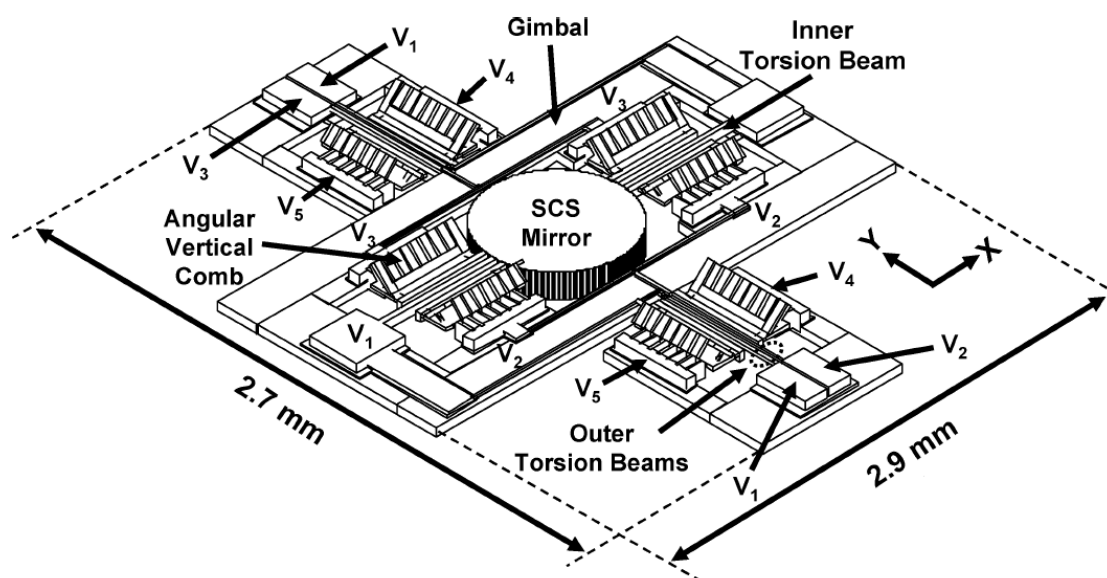

Fig. 3.14. Schematic of 2D AVC gimbal scanner (Reprinted from [58] with permission).

The endoscope head is 5-mm in diameter and 2.5-cm long, which is compatible with requirements for minimally invasive endoscopic procedures. Figure 3-15 shows a schematic of the fiber coupled MEMS scanning endoscope. The compact aluminum housing can be machined for low cost and allows precise adjustment of optical alignment using tiny set screws. The optics consists of a graded-index fiber collimator followed by an anti-reflection coated achromatic focusing lens producing a beam diameter of ~ 12 um [56,57].

The 2D MEMS scanner is mounted at 45 degrees and directs the beam orthogonal to the endoscope axis in a side-scanning configuration similar to those typically used for endoscopic OCT procedures. Post-objective scanning eliminates off-axis optical aberration encountered with pre-objective scanning. Figure 3-16 shows a scanning electron micrograph of the 2D AVC scanner located inside the endoscope package. The large 1-mm diameter mirror allows high-numerical-aperture focusing.
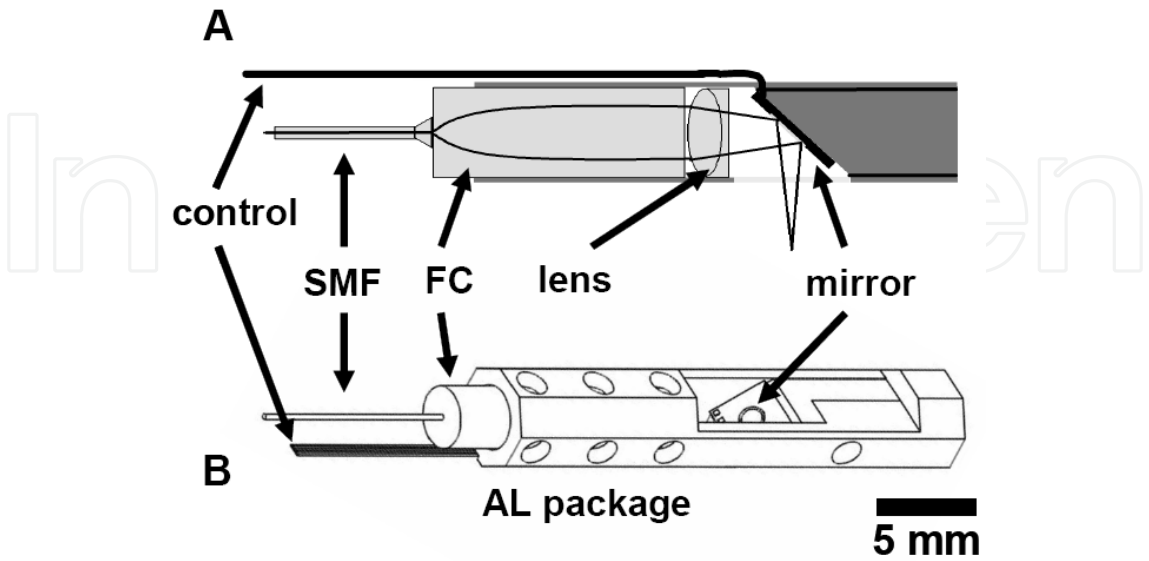
Fig. 3.15. Schematic drawing of the endoscope head (Reprinted from [56] with permission).
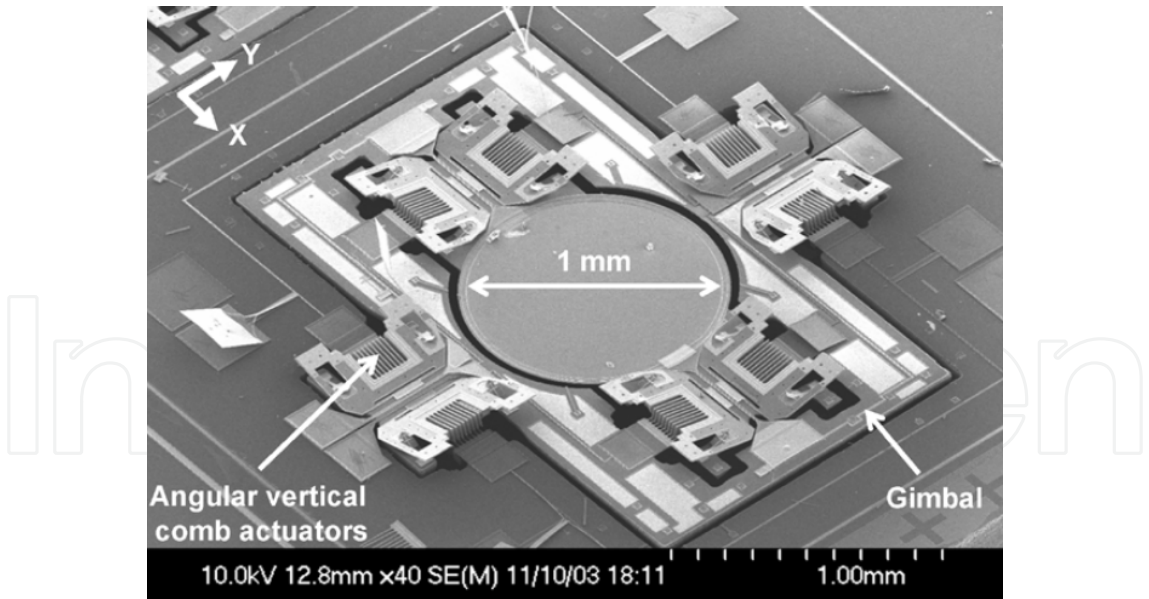

Fig. 3.16. SEM of 2D AVC gimbal scanner (Reprinted from [58] with permission).

Recently, Huikai Xie et. al developed a miniature endoscopic optical coherence tomography probe system employing a two-axis microelectromechanical scanning mirror with through-silicon vias (TSV). The new scanner's design (Figure 3-17) improves the assembly and package of the probe.
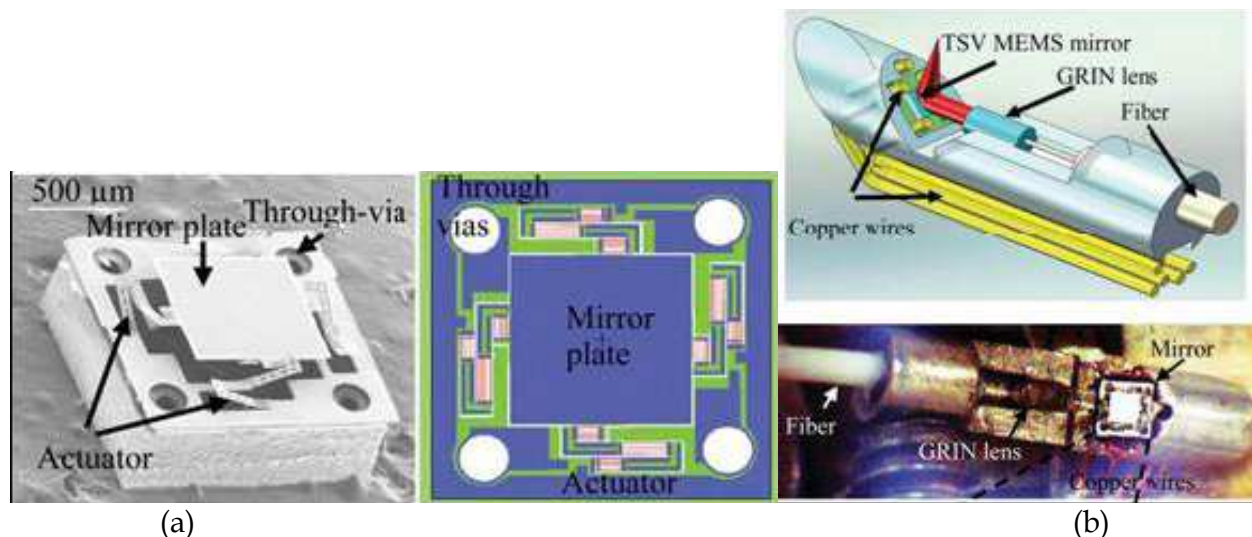
Fig. 3.17. Electrothermal MEMS OCT reported by Liu et al. (a) SEM and schematic of through vias electrothermal MEMS mirror, (b) 2.6mm probe 3D model and assembled probe, (Picture courtesy of Huikai Xie. Reprinted from [18] with permission).

3.1.5 Adaptive optics

Optical MEMS devices offer a promising alternative to piezoelectric and other deformable mirror types used in adaptive optics applications. Adaptive optics refers to optical systems which adapt to compensate for undesirable optical effects introduced by the medium between the object and its image. It provides a means of compensating for these effects, leading to appreciably sharper images approaching the theoretical diffraction limit. These efforts include wave front correction, aberration cancellation etc. While sharper images come with an additional gain in contrast for astronomy, where light levels are often very low, this means fainter objects can be detected and studied [60, 61]. Other interesting applications used adaptive optics are confocal microscopy [62], adaptive laser wavefront correction [63], cryogenic adaptive optics [64], and human vision [65]. Several groups have developed MEMS deformable mirrors.

A two-level silicon surface micromachining approach was employed by researchers at Boston University to produce MEMS deformable mirrors using an original architecture described in Figure 3-18 [66,67]. The kilo-pixel spatial light modulator is made up of 1024 individually addressable surface-normal electrostatic actuators with center posts that support individual optical mirror segments. Each electrostatic actuator consists of a silicon membrane anchored to the substrate on two sides above a silicon electrode. These devices were manufactured at a commercial MEMS foundry [68]. A post centered on each actuator supports a 338μm x 338μm x 3μm optically coated mirror segment. The spatial light modulator has an aperture of 10 mm, an actuator stroke of 2 μm, and a position repeatability of 3 nm. The resonant frequency of the mirror is around 60 kHz.

At Jet Propulsion Laboratory (JPL), researchers developed a single crystal silicon continuous membrane deformable mirror with underlying piezoelectric unimorph actuators as shown in Figure 3-19 [69]. A PZT unimorph actuator of 2.5 mm in diameter with optimized PZT/Si thickness and design showed a deflection of 5 μm at 50V. Deformable mirrors consisting of 10μm thick single-crystal silicon membranes supported by 4×4 actuator arrays were

fabricated and optically characterized. An assembled deformable mirror showed a stroke of 2.5μm at 50V with a resonant frequency of 42 kHz.
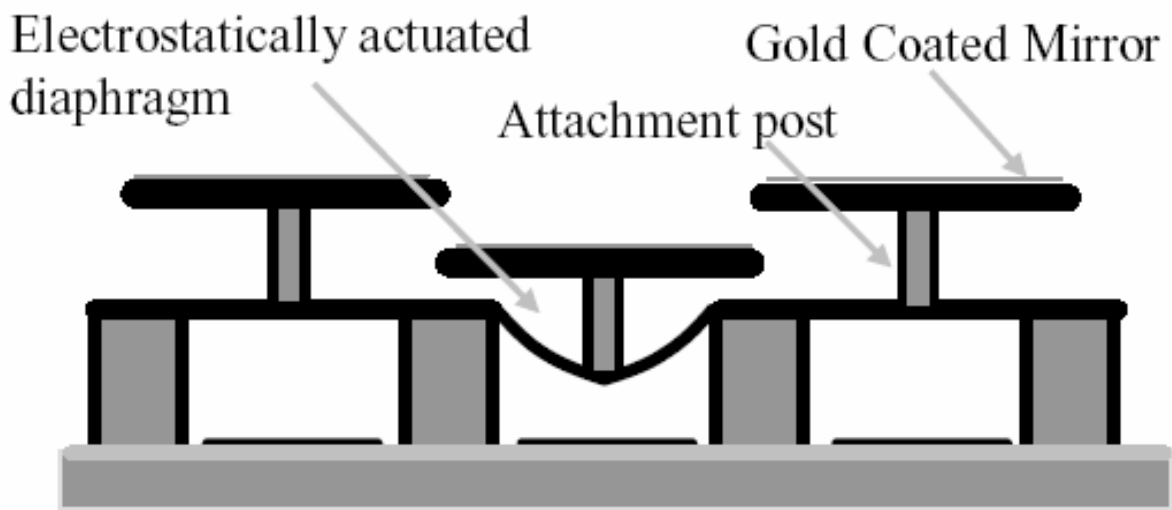

Fig. 3.18. Schematic cross section of a gold coated spatial light modulator with a central deflected actuator (Picture courtesy of Thomas G. Bifano. Reprinted from [66] with permission).

Fig. 3.19. Cross-sectional drawing of the deformable mirror
(Reprinted from [69] with permission).

Another MEMS adaptic optical system has been developed by IRIS AO Inc. [70] using Au-coated dielectric-coated segmented MEMS deformable mirrors (DM) for Optical MEMS application. The AO system (Figure 3-20) consists of piston-tip-tilt (PTT) segmented MEMS deformable mirrors (DM) and adaptive optics controllers for these DMs, shown in Figure 3-20. Researchers from IRIS AO Inc. have made many improvements for mirrors to realize open-loop flatten up to 4 nm rms.

<p style="text-align:center">(a)   (b)</p>

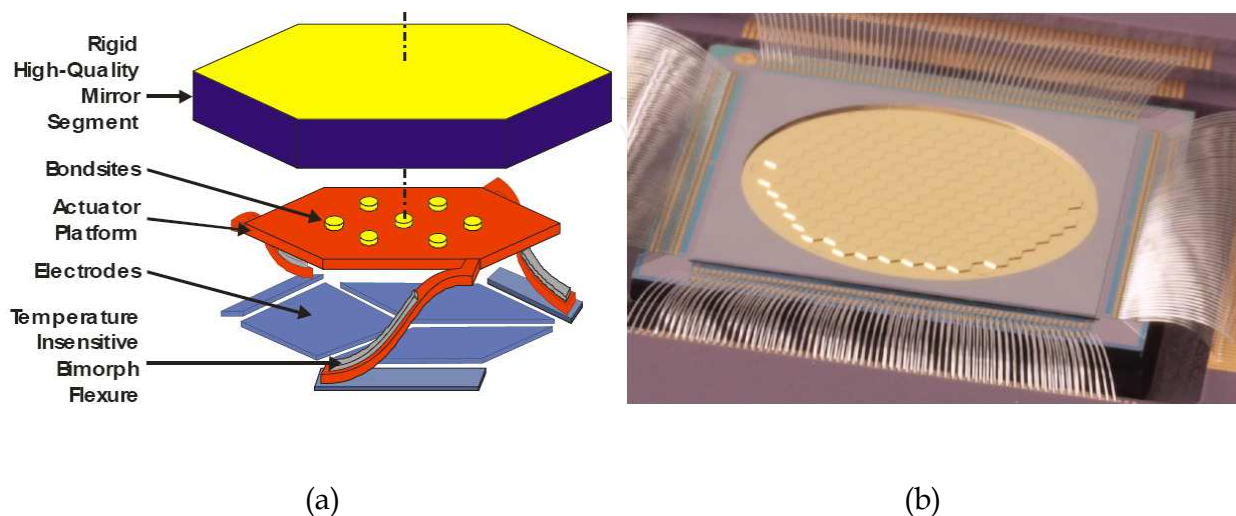Fig. 3.20. a) Schematic diagram of a 700 µm diameter (vertex-to-vertex) mirror segment. Scaling is highly exaggerated in the vertical direction. b) Die photograph of a 489-actuator 163-piston/tip/tilt-segment DM with 7.7 mm inscribed aperture (Product name: PTT489-5). (Reprinted from [70] with permission).

3.1.6 Other examples

Researchers at UCLA fabricated two cascaded two dimensional scanners for optical surveying instruments [71]. Currently, cascaded acousto-optic deflectors are used the optical surveying instruments. MEMS scanners are very attractive candidates for replacing those scanners. They offer many advantages, including lower power consumption, smaller size, and potentially lower cost. Optical surveying instruments require mirrors with reasonably large scan range (~ ±6° mechanical), high resonant frequencies (5-10 kHz for fast axis), large radius of curvature, and low supply voltage (< 50V).

Typically, the target, a highly reflective surface consisting of corner cubes, is located several meters to several kilometers away from the instruments. The required scanning angular range is relatively small, on the order of a few degrees. The angular divergence of the measurement laser beam is typically a few milliradians or narrower. Hence the target search system needs to resolve several tens of spots in the entire scan range. Raster scanning has been used because the laser beam needs to search the entire area within the field of view to find the target. A combination of fast and slow scanning scanners has been employed. Both are fabricated by using bulk micromachining technique with 25-µm-thick SOI wafer. The fast scanner has a circular shape and achieved a resonant frequency of 7.5 kHz with the maximum mechanical rotation in DC mode of ±3.2 degrees. The slow scanner has an elongated circular shape and achieved a resonant frequency of 1.2 kHz with the maximum mechanical rotation in DC mode of ±0.74 degree. Figure 3-21 shows the SEM of the fast mirror.
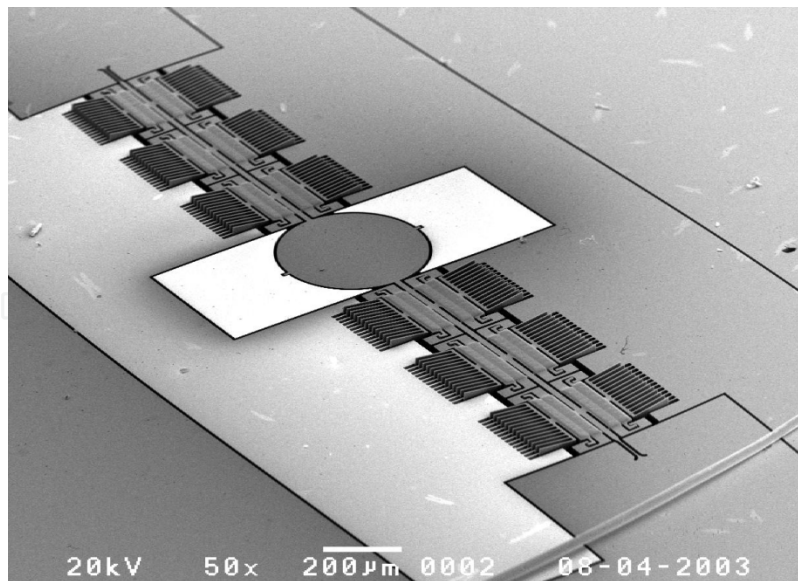
Fig. 3.21. SEM of the fast mirror (Reprinted from [71] with permission)

3.2 Optical communication
3.2.1 2D MEMS switch

The two-dimensional (2D) MEMS optical switch is basically an optical crossbar switch with N^2 micromirrors that can selectively reflect the optical beams to orthogonal output ports or pass them to the following mirrors. They are often referred to as "2D switches" because the optical beams are switched in a two-dimensional plane. This is in contrast to the 3D switch (discussed in the following section) in which the optical beams are steered in three-dimensional space. A generic configuration of the 2D switch is shown in Figure 3-22. The core of the switch is an NxN array of micromirrors for a switch with N input and N output fibers. The optical beams are collimated to reduce diffraction loss. The micromirrors intersect the optical beams at 45°, and can be switched in and out of the optical beam path. The micromirrors are "digital", that is, they are either in the optical beam path (ON) or completely out of the beam path. When the mirror in the i-th row and j-th column (M_{ij}) is ON, the i-th input beam is switched to the j-th output fiber. Generally, only one micromirror in a column or a row is ON. Thus during operation of an NxN switch, only N micromirrors are in the ON position while the rest of the micromirrors are in the OFF position. MEMS 2D switches were first reported by Toshiyoshi and Fujita [72]. Several different ways of switching micromirrors have been reported, including rotating, sliding, chopping, and flipping motions. The switches are usually actuated by electrostatic, electromagnetic, or piezoelectric mechanisms.

2D switches using various types of flip-up (or pop-up) mirrors have been reported [72,73,74,75]. They are realized by either the bulk- [72] or the surface-micromachining [73] technology, or the combination of both [74]. The mirror lies in the plane of the substrate during OFF state and pops up in the ON state. Since the mirror angle is changing continuously during switching, a common challenge for this type of switch is the reproducibility of mirror angle. This is a critical issue as the mirror angles and their uniformity play a critical role in the performance and the scalability of 2D switches. The reproducibility of mirror angles over switching cycles determines the repeatability of insertion loss.
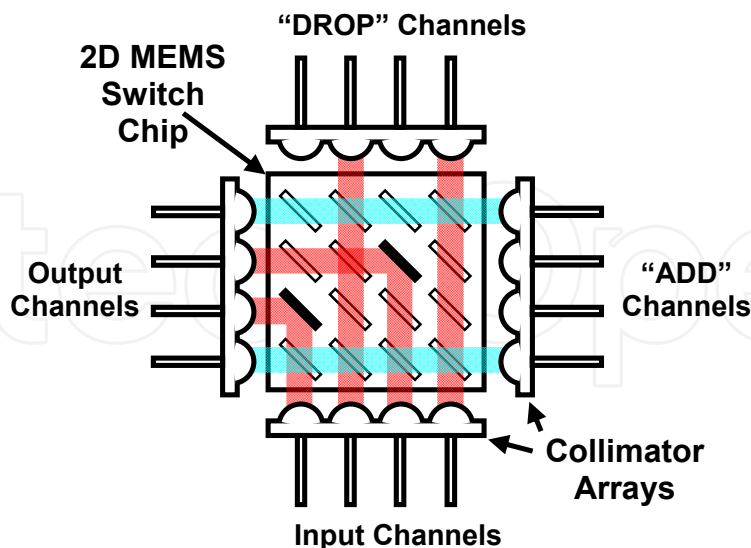
Fig. 3.22. Schematic of 2D MEMS optical switches.

The first 2D matrix optical switch reported by Toshiyoshi and Fujita employed pop-up-type switching elements, as shown in Figure 3-23 [72]. It consists of two bonded wafers. The mirrors are suspended by a pair of torsion beams in the plane of the top wafer. The biasing electrodes are fabricated on the bottom wafer. When a voltage is applied between the mirror and the bottom electrode, the mirror rotates downward by 90° by electrostatic actuation. The mirror angle in the ON (down) state is controlled by a stopper on the bottom wafer. Since the mirror angle is defined by the relative positions of two wafers, precise alignment is necessary to achieve accurate and uniform mirror angles. A single-chip electrostatic pop-up mirror has recently been reported [76]. The actuation and mechanical stopper are realized between a back-flap and a vertical trench etched in the silicon substrate. The angular accuracy and uniformity of their mirrors depend on the etched sidewall profile and the lithographic alignment accuracy.

AT&T Lab has reported surface-micromachined 2D switches with free-rotating hinged mirrors [73,77,78]. The schematic drawing and the SEM of the switch are shown in Figure 3-24. It is fabricated using the MUMPs process. The mirror is pivoted on the substrate by microhinges. A pair of pushrods is used to convert in-plane translations into out-of-plane rotations of the mirrors. The switch is powered by scratch drive actuators [79]. Though scratch drive actuators do not move at high speed, fast switching time is achieved (700 μsec) because only a short traveling distance (22 μm) is needed for the mirror to reach 90°. The free-rotating microhinges have an inherent 0.75-μm clearance between the hinge pins and the staples, which could result in large variations in mirror angles. Using improved design and mechanical stoppers that are insensitive to lithographic misalignment during fabrication, mirror angular repeatability of better than 0.1° was experimentally demonstrated [80]. The mirror flatness was improved by using a multi-layer structure with phosphosilicate glass (PSG) sandwiched between two polysilicon layers. The largest switch size demonstrated is 8x8 due to the foundry-imposed chip-size limits of 1 cm x 1 cm. One of the potential issues is the constant tear and wear of the free-rotating hinges and actuators.

This might affect the reliability of the switch and the accuracy and uniformity of mirror angles over many switching cycles.

TORSION MIRROR CHIP

MIRROR is ON

M₄

MIRROR is OFF

M₁   M₃

M₂

SPHERICAL LENS

MIRROR STOPPER
(SHALLOW DIMPLE)

3mm

COUNTER ELECTRODE

COUNTER ELECTRODE

TORSION MIRROR

GROOVE
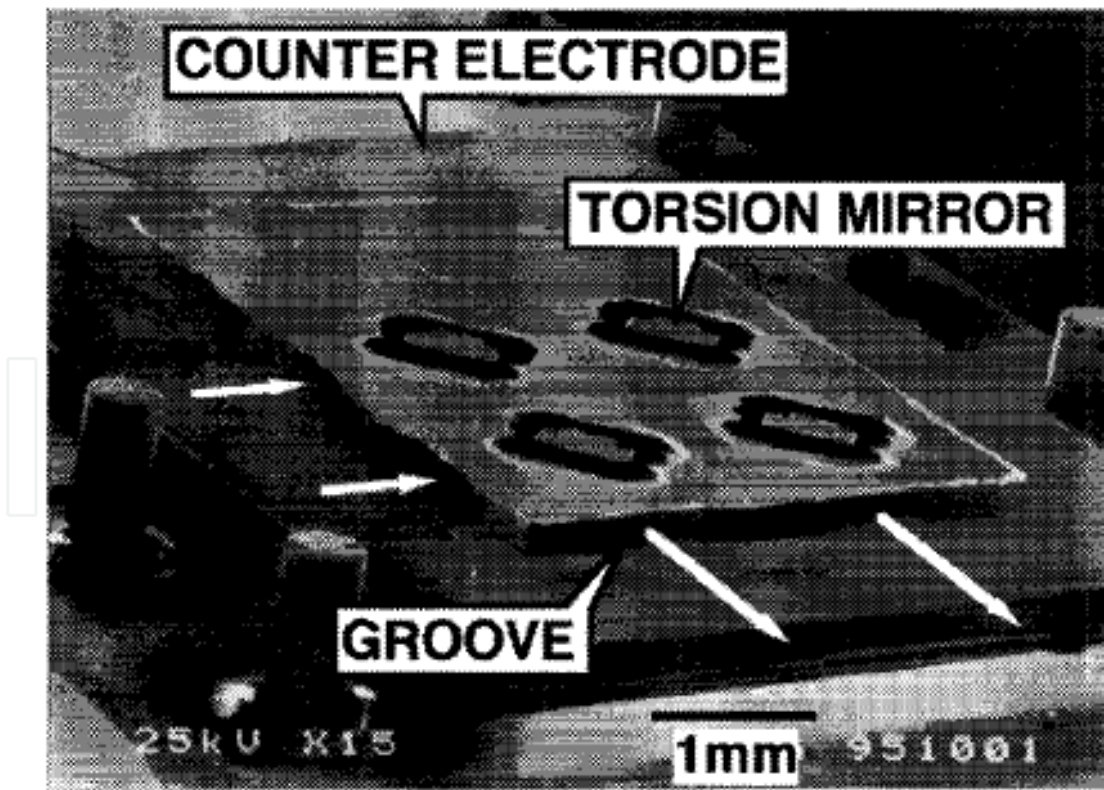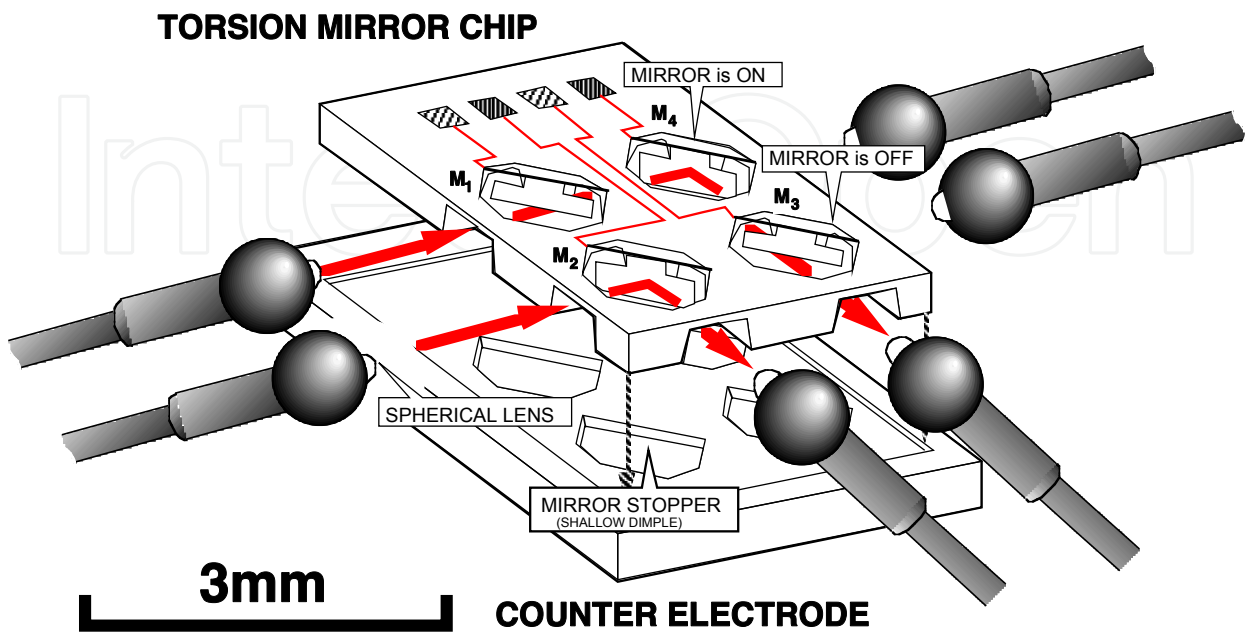
25kV X15   1mm 951001

Fig. 3.23. Schematic and SEM of bulk-micromachined 2D switch with free-rotating torsion mirrors (Pictures courtesy of Hiroshi Toshiyoshi. Reprinted from [72] with permission).
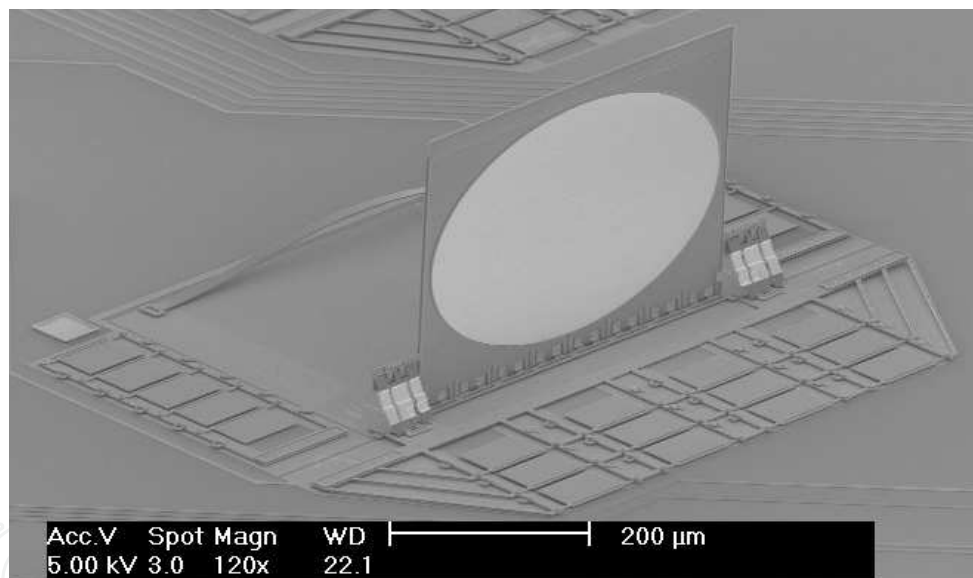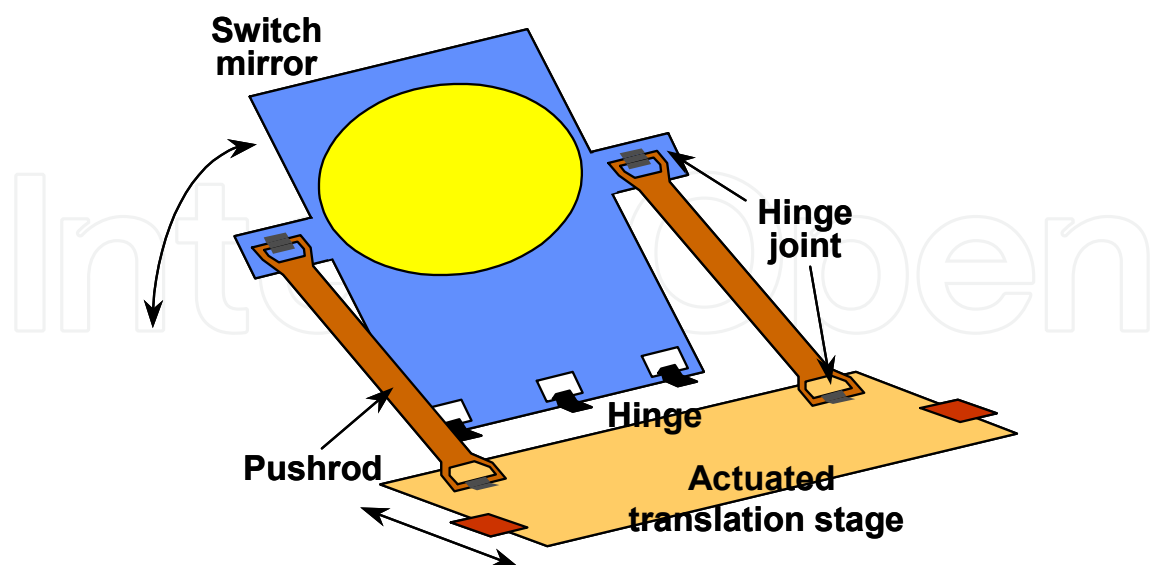
Fig. 3.24. Schematic and SEM of the surface-micromachined free-rotating hinged mirrors reported by AT&T (Picture courtesy of Lih Y. Lin. Reprinted from [73,77] with permission).

On the other hand, the "chopper type" 2D switch employs a vertical mirror whose height can be changed by MEMS actuators [81,82]. The mirror angle is fixed during switching, and excellent repeatability of insertion loss has been reported. Figure 3-25 shows the schematic diagram of OMM's 2D switch [81]. The mirror is assembled vertically at the tip of a long actuator plate. The plate is tilted upward and fixed by micro-latches to raise the mirror height. Large traveling distance is achieved by extending the actuator arm. Several hundred microns displacement can be achieved with this configuration. The switch is actuated electrostatically by applying a voltage between the actuator plate and a bottom electrode on the substrate. The mirror moves in the vertical direction and the mirror angle

is maintained at 90° during the entire switching cycle. The actuator is basically a gap-closing actuator. A mechanical stopper defines the lower position of the mirror. OMM employs a curved landing bar with a single point contact to minimize stiction and increase reliability (see Figure 3-25). More than 100 million cycles have been demonstrated with repeatable mirror angle and performance. The landing bar also provides a cushion that helps reduce mirror ringing and improve switching time. They have demonstrated a switching time of 12 ms using a square-wave driving voltage without pre-shaping the waveform. OMM's switch is fabricated with polysilicon surface-micromachining technology. The mirrors and the actuators are batch-assembled into the 3D structures. Figure 3-26(a) shows the SEM of a 16x16 switch. The distribution of mirror angles is shown in Figure 3-26(b). The uniformity is better than ±0.1 degrees for 256 mirrors. The switch is hermetically packaged with optical collimator arrays. Extensive testing has been performed for the packaged switches. The maximum insertion loss is less than 3.1 dB and the crosstalk is less than – 50 dB. Loss variation over the wavelength range of 1280 – 1650 nm range is less than1 dB. Return loss is greater than 50dB, and maximum temperature variation is < 1 dB over a temperature range of 0 - 60°C. Polarization dependent loss (PDL) is < 0.4 dB and polarization mode dispersion (PMD) is < 0.08 ps. Vibration tests show < 0.2 dB change under operation, and 3 axis shock tests confirm no change of operational characteristics under 200 G.
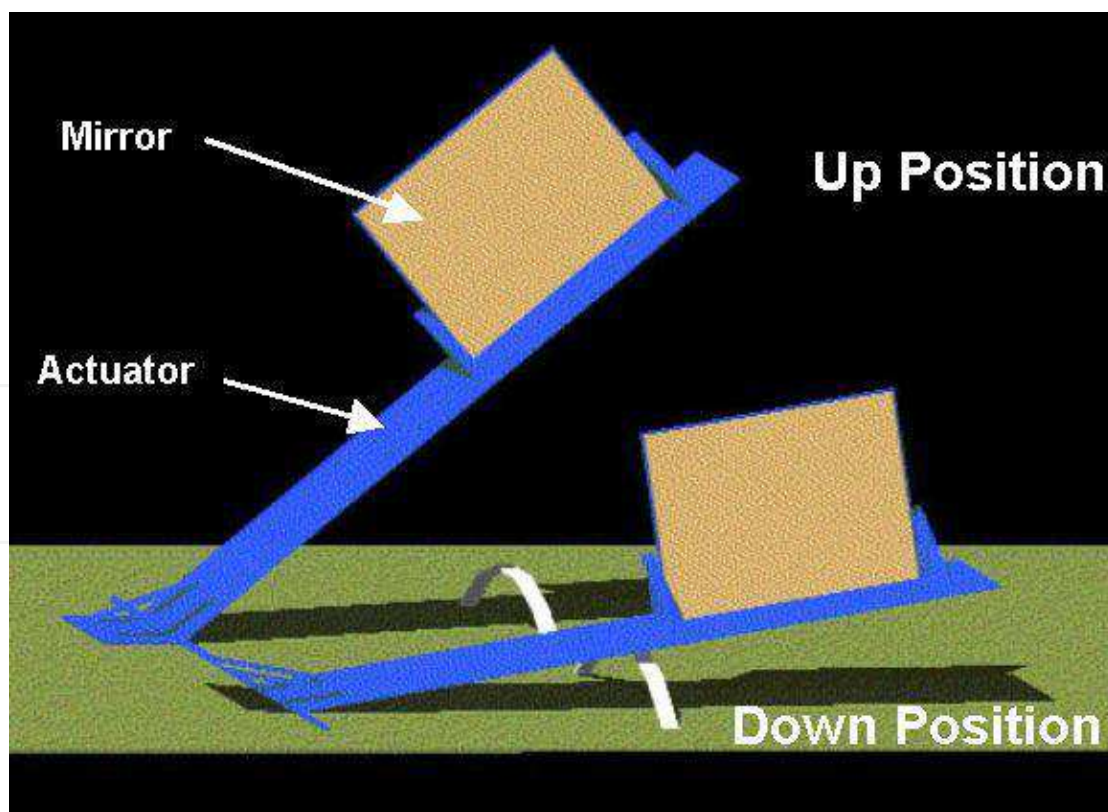

Fig. 3.25. Schematic of a switching element in OMM's 2D switch (Picture courtesy of Li Fan. Reprinted from [81] with permission).
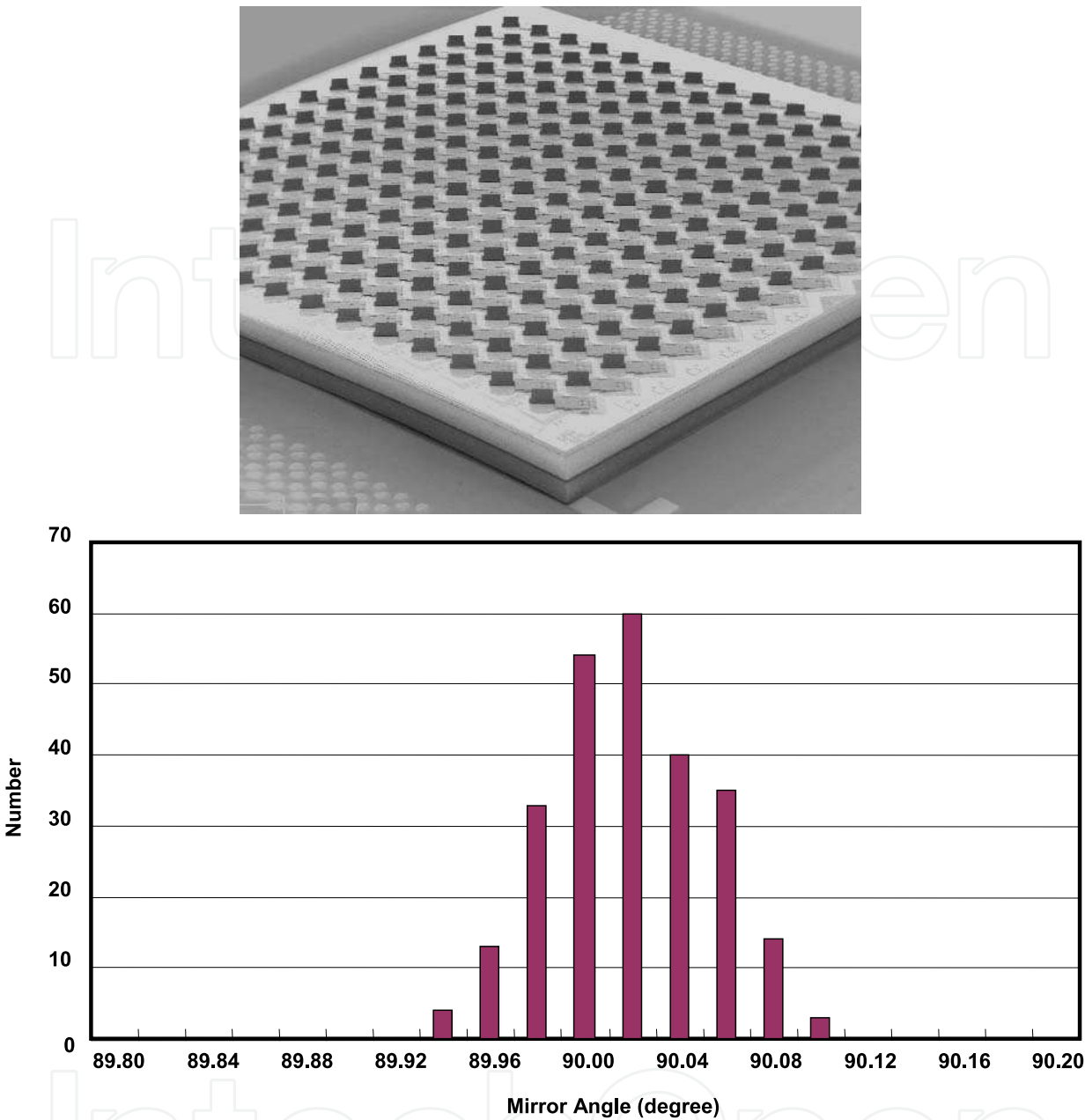
Fig. 3.26. (a) SEM of OMM's 16x16 switch. (b) Measured distribution of mirror angles for the 16x16 switch (Picture courtesy of Li Fan. Reprinted from [81] with permission).

The structure of a 2x2 2D MEMS switch can eventually be simplified so that it requires only one single micromirror between two pairs of orthogonal fibers. A simple, elegant solution for 2x2 switches is using SOI-based Optical MEMS [83,84]. The schematic and SEM picture (only fiber grooves shown) of the 2x2 switch are shown in Figure 3-27. Electrostatic comb drive actuators and vertical micromirrors are fabricated on 75-μm SOI wafers. The mirrors can be coated with metal by angle evaporation to increase their reflectivity. The most critical part of the process is the etching of thin (< 2 μm) vertical mirrors with smooth sidewalls. Thin vertical mirror is required for such a 2x2 switch because the offset of the reflected optical beams from the opposite sides of the mirror caused by the finite thickness of the mirror will introduce additional optical loss. The Institute of Microtechnology (IMT) at

Neuchatel has perfected the mirror etching technology by DRIE [85]. A surface roughness of 36 nm has been achieved. The switch has excellent optical performance: 0.3-0.5 dB optical insertion loss and 500 μsec switching time, and very low polarization dependence [84].
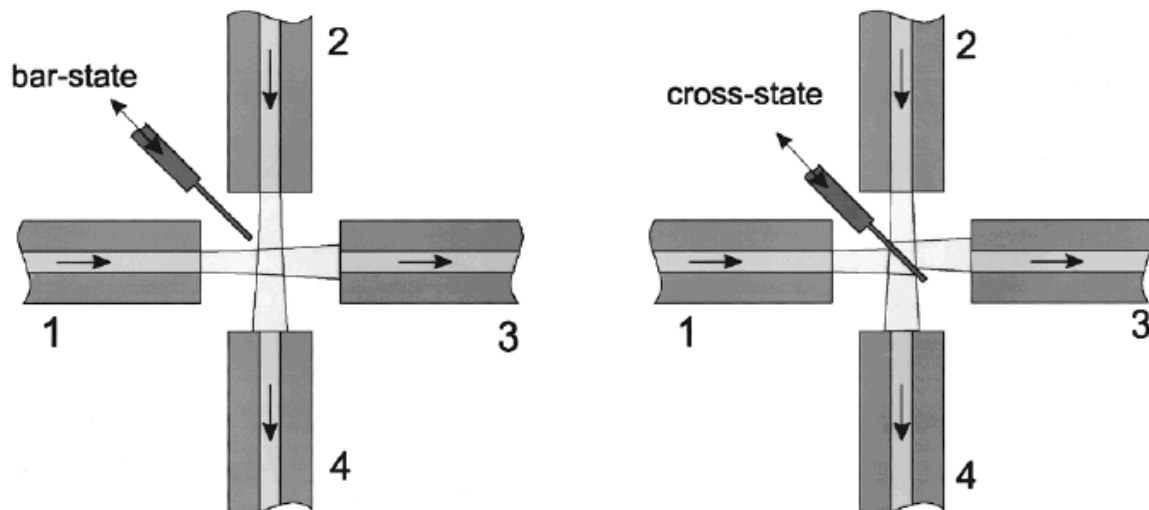

Fig. 3.27. Schematic and SEM of 2x2 switch fabricated by SOI MEMS (Picture courtesy of Nico de Rooij. Reprinted from [83] with permission).

3.2.2 3D MEMS switch

Telecommunication switches with large port count have been the main driver for the two-axis scanner in the past few years. With increasing number of wavelengths and bandwidth in dense wavelength-division-multiplexed (DWDM) networks, there is a need for optical crossconnect (OXC) with large port count [86,87,88]. The dual axis analog scanning capability is the key for these applications since each mirror associated with the input fiber array can point to any mirror associated with the output fiber array. Implementation of NxN OXC using two arrays of N analog scanners is illustrated in Figure 3-28. Even though the implementations may vary, we can always conceptually refer to this illustration. This switch is often called a 3D MEMS switch because the optical beams propagate in three-dimensional space. 3D switch is a better choice for larger port-count NxN OXC compared to 2D switch as the number of mirrors for a 2D switch is N^2. Since the optical path length is independent of the switch configuration, uniform optical insertion loss (2 to 3 dB) can be achieved. The port count of the 3D MEMS switch is limited by the size and flatness of the micromirrors, as well as their scan angle and fill factor. For a complete discussion of scaling laws for MEMS free space optical switches, see Syms [88]. For large port count (approaching 1000 x 1000), single crystal micromirror scanners are necessary to achieve large mirror size with required flatness.

During the telecom boom, several companies have invested heavily to develop 3D MEMS OXC's. These companies include (but not limited to) Lucent Technologies [86,88,89,90,91,92,93,94], Corning [95,96,97], NTT Corp. [98,99], Fujitsu Laboratories, Ltd. [100,101], Tellium, Inc. [102,103,104], and Calient Networks [105]. They have demonstrated various designs of two-axis scanners, which are the key components of these 3D MEMS switches.

Fig. 3.28. Configuration for 3-D optical switch (NxN) with 2N analog scanning mirrors.

Lucent technologies employed a self-assembly technique which was driven by the residual stress in deposited thin films (Cr/Au on polysilicon) to raise two-axis polysilicon scanners (500 μm mirror diameter) to a fixed position 50 μm above the substrate [106,107]. The scanning electron micrograph (SEM) is shown in Figure 3-29. Two-axis scanning is achieved

Fig. 3.29. SEM of surface-micromachined 2-axis scanners Lucent Technologies (Courtesy of [109] Lucent Technologies Inc. © 2003 Lucent Technologies Inc. All rights reserved.)

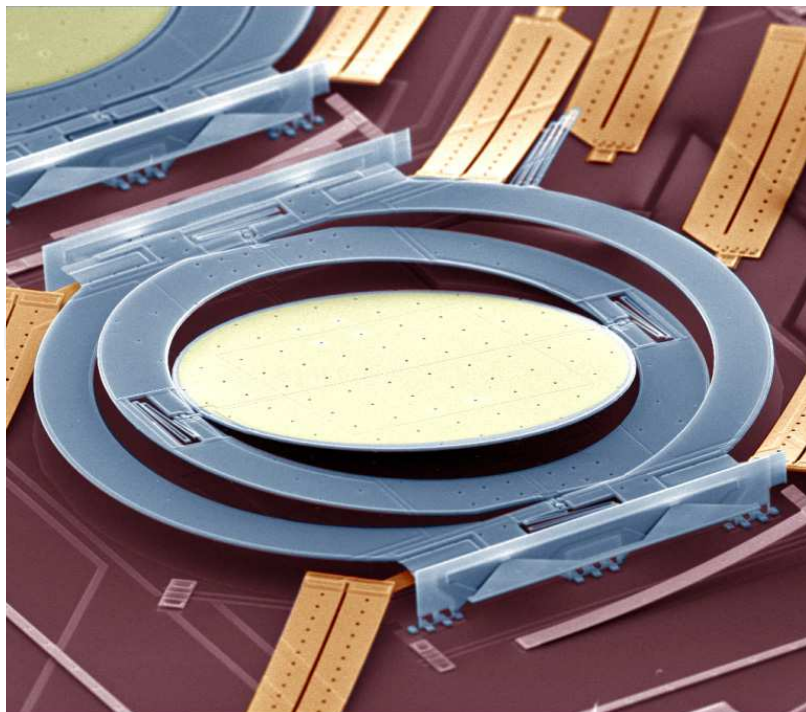by electrostatic force between the mirror and the quadrant electrodes on the substrate. SCS two-axis scanner with long-term stability and high shock resistance has also been developed by Lucent Technologies for 3D MEMS switches [108, 109]. SCS is used to improve the mirror flatness. The long-term stability is achieved by the removal of exposed dielectric to avoid electrostatic charge-up effect (Figure 3-30). The scanning angle is 7 degrees.
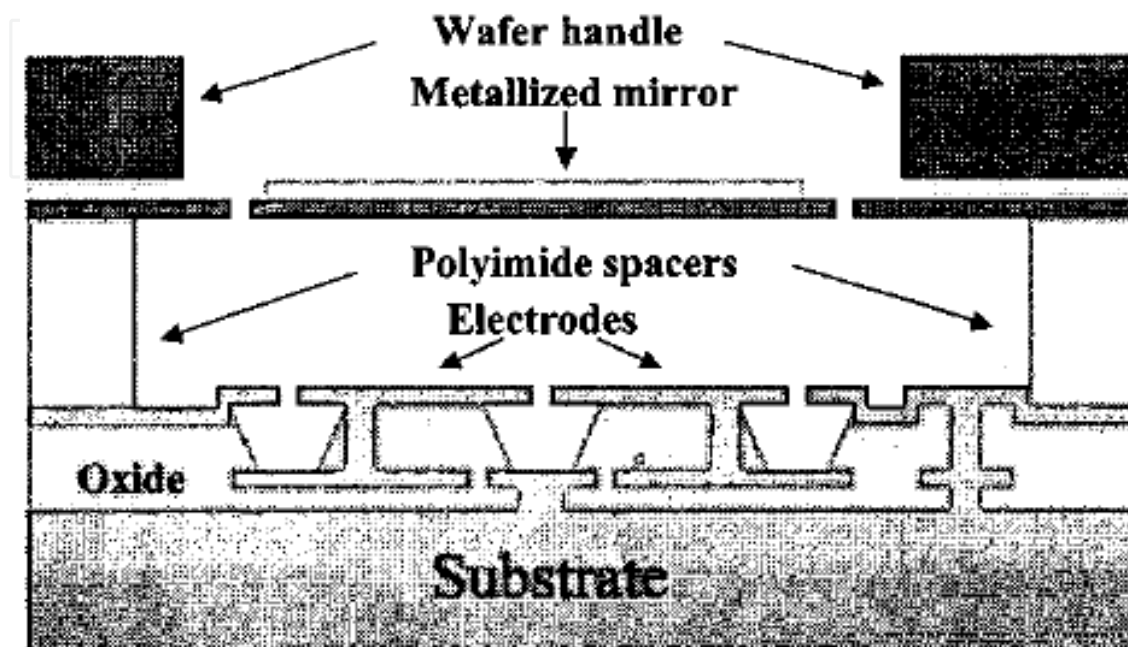

Fig. 3.30. Cross section of the SCS two-axis mirror developed by Lucent Technolgies (Picture courtesy of A. Gasparyan. Reprinted from [108] with permission)

NTT Corp. has reported a two-axis micromirror array driven by terraced electrodes. The mirrors and the electrodes are fabricated on separate chips and then bonded together. The use of terraced electrodes reduces the applied voltage by half, compared to regular parallel-plate-driven mirrors. The mirror is tilted by 5.4 degree at a maximum of 75 V. The resonant frequency of the fabricated mirror is approximately 1 kHz [98].

The two-axis scanner developed by Fujitsu Laboratories, Ltd. is based on vertical comb-drive actuators. SOI with 100-μm top and bottom (substrate) silicon layers has been used to fabricate the device [100]. The top silicon is for the moving comb fingers and mirror while the fixed fingers are made of the bottom silicon. V-shape torsion springs are adopted to improve the lateral stability which is a critical issue in comb-drive actuators. Rotation angle of +/- 5 degrees has been achieved with 60-V driving voltage.

Tellium, Inc. has demonstrated an electrostatic parallel-plate actuated two-axis scanner, featuring nonlinear servo closed-loop control [102]. The nonlinear servo closed-loop control enables the mirror to operate beyond the pull-in angle. Figure 3-31 shows the comparison of switching under open-loop and closed-loop operation. The closed-loop angular trajectory can exceed the pull-in (snap-down) angle and shows no overshoot. They have also developed a two-axis micromirror driven by both sidewall and bottom electrodes [104]. The addition of sidewall electrodes improves the linearity of the DC transfer characteristic. The mirror with sidewall electrodes also exhibits a larger scan angle than that driven by merely bottom electrodes (Figure 3-32).

Fig. 3.31. Comparison of switching under open-loop and closed-loop operation (Picture Reprinted from [102] with permission)

Fig. 3.32. DC transfer characteristics of the two-axis scanner of Tellium, Inc., with and without sidewall driving (Picture courtesy of C. Pu. Reprinted from [104] with permission)

4. Conclusion

In this Chapter, we present the history, common actuators, and fabrications of various Optical MEMS devices for display, imaging, and telecom applications. Each actuation mechanism has its own advantage that can be optimally deployed in each application. For instance, electrostatic actuation requires very low current and achieves short range in motion suiting

for low power consumption application. In contrast, magnetic actuation needs high current (implying high power) and achieves long range in motion which is suitable for long range actuation application with less constraints on current driving limit.

The Optical MEMS technology promises to revolutionize nearly every product category with the ability to directly manipulate light or optical signal. With the integration of microelectronics and microoptical components, it is the possible realization of complete systems on a chip.

5. References

[1] Petersen, K. E., "Silicon torsional scanning mirror," IBM J. R&D, vol. 24, pp.631-7, 1980.

[2] M.C. Wu, "Micromachining for Optical and Optoelectronic Systems," Proc. IEEE, Vol. 85 (IEEE Press, Piscataway, N.J., 1997), pp. 1833–1856.

[3] R.S. Muller and K.Y. Lau, "Surface-micromachined microoptical elements and Systems," Proc. IEEE, Vol. 86, (IEEE Press, Piscataway, N.J., 1998), pp.1705-1720.

[4] Degani, O., Socher, E., Lipson, A., Leitner, T., Setter, D. J., Kaldor, S., and Nemirovsky, Y., "Pull-In Study of an Electrostatic Torsion Microactuator," IEEE J. Microelectromech. Syst., vol. 7, no. 4, pp. 373-379, 1998.

[5] Hah, D., Toshiyoshi, H., and Wu, M.C., "Design of Electrostatic Actuators for MOEMS," Proc. SPIE, Design, Test, Integration and Packaging of MEMS/MOEMS 2002, May 2002, Cannes, France

[6] R. A. Conant, J.T. Nee, K. Lau, R.S. Mueller "A Flat High-Frequency Scanning Micromirror", 2000 Solid-State Sensor and Actuator Workshop, Hilton Head, SC, pp. 6-9.

[7] P. R. Patterson, D. Hah, H. Chang, H. Toshiyoshi, M. C. Wu, "An Angular Vertical Comb Drive for Scanning Micromirrors", IEEE/LEOS International Conference on Optical MEMS, Sept. 25-28, 2001, Okinawa, Japan, p.25

[8] Schenk, H., Durr, P., Haase, T., Kunze, D., Sobe, U., Lakner, H., Kuck, H., "Large deflection micromechanical scanning mirrors for linear scans and pattern generation", Selected Topics in Quantum Electronics, IEEE Journal of, Sep/Oct 2000, vol. 6 Issue:5, pp. 715 – 722

[9] Sandner, T., Jung, D., Kallweit, D., Grasshoff, T., Schenk, H., "Microscanner with vertical out of plane combdrive", Optical MEMS and Nanophotonics (OMN), 2011 International Conference on Issue Date: 8-11 Aug. 2011, Istanbul, Turkey, pp. 33 - 34

[10] Judy, J.W. and Muller, R.S., "Magnetically Actuated, Addressable Microstructures," IEEE J. Microelectromech. Syst., vol. 6, no. 3, pp. 249-256, 1997.

[11] H. Miyajima et al., "A MEMS electromagnetic optical scanner for a commercial confocal laser scanning microscope," Journal of Microelectromechanical Systems, Vol. 12, No. 3, pp. 243-251, Jun. 2003.

[12] Il-Joo Cho, Euisik Yoon, "A low-voltage three-axis electromagnetically actuated micromirror for fine alignment among optical devices", Journal of Micromechanics and Microengineering vol. 19, no. 8, Aug. 2009.

[13] A. Jain, et al., "A two-axis electrothermal SCS micromirror for biomedical imaging", 2003 IEEE/LEOS International Conference on Optical MEMS 3, pp.14-15.

[14] Ankur Jain, Hongwei Qu, and Shane Todd, Gary K. Fedder, and Huikai Xie, "Electrothermal SCS micromirror with large-vertical-displacement actuation," 2004 Solid-State Sensor and Actuator Workshop Tech. Digest, June 2-6, Hilton Head, SC, pp.228-231.

[15] Lei Wu, Huikai Xie, "A large vertical displacement electrothermal bimorph microactuator with very small lateral shift" Sensors and Actuators A: Physical, vol 145-146, July-August 2008, pp. 37

[16] Lei Wu, Dooley, S., Watson, E.A., McManamon, P.F., Huikai Xie, "A Tip-Tilt-Piston Micromirror Array for Optical Phased Array Applications" Microelectromechanical Systems, Journal of, vol. 19 Issue:6, pp. 1450 – 1461, Dec. 2010

[17] Jingjing Sun, Shuguang Guo, Lei Wu, Lin Liu, Se-Woon Choe, Brian S. Sorg, and Huikai Xie, "3D In Vivo optical coherence tomography based on a low-voltage, large-scan-range 2D MEMS mirror", Optics Express, Vol. 18, Issue 12, pp. 12065-12075 (2010)

[18] Jingjing Sun, Huikai Xie, "MEMS-Based Endoscopic Optical Coherence Tomography" International Journal of Optics, vol 2011 (2011), Article ID 825629, 12 pages

[19] Zhen Qiu, Jeffrey S Pulskamp, Xianke Lin, Choong-Ho Rhee, Thomas Wang, Ronald G Polcawich and Kenn Oldham, "Large displacement vertical translational actuator based on piezoelectric thin films", 2010 J. Micromech. Microeng. 20 075016

[20] Holger Conrad, Jan Uwe Schmidt, Wolfram Pufe, Fabian Zimmer, Thilo Sandner, Harald Schenk, Hubert Lakner, "Aluminum nitride: a promising and full CMOS compatible piezoelectric material for MOEMS applications", Proc. SPIE 7362, 73620J (2009)

[21] Holger Conrad, Wolfram Pufe and Harald Schenk, "Aluminum Nitride Thin Film Development using Statistical Methods", 2011 International Students and Young Scientists Workshop „Photonics and Microsystems

[22] H.-J. Nam, Y.-S. Kim, S.-M. Cho, Y. Yee, and J.-U. Bu, "Low Voltage PZT Actuated Tilting Micromirror with Hinge Structure," 2002 IEEE/LEOS International Conference on Optical MEMS, Lugano, Switzerland, pp.89-90

[23] Bourouina,T., Lebrasseur,E., Reyne,G., Debray,A., Fujita, H., Ludwig, A., Quandt, E., Muro, H., Oki, T., and Asaoka, A., "Integration of Two Degree-of-Freedom Magnetostrictive Actuatio and Piezoresistive Detection: Application to a Two-Dimensional Optical Scanner," IEEE J. Microelectromech. Syst., vol. 11, no. 4, pp. 355-361, 2002.

[24] L. J. Hornbeck, "Digital Light Processing™ for High Brightness, High Resolution Applications," Proc. SPIE vol. 3013 (Electronic Imaging EI'97, Feb. 10-12, 1997, San Jose, CA).

[25] See for example, S. Senturia, Microsystem Design, Chapter 20, Kluwer Academic Publishers, 2001

[26] The Perspectra® product from Actuality Systems

[27] Z20/20™ product from VIZTA3D

[28] UV-Setter™ print-setting product from BasysPrint GmbH

[29] M. Liang, R. L. Stehr, A.W. Krause, "Confocal pattern period in multiple aperture confocal imaging systems with coherent illumination, Opt. Lett. 22, pp. 751-753, 1997

[30] C. MacAulay, A. Dlugan, Use of digital micro mirror devices in quantitative microscopy, Proc. SPIE Vol. 3260, 1998, pp. 201.

[31] A.L.P. Dlugan, C. E. MacAulay, and P.M> Lane, "Improvements to quantitative microscopy through the use of digital micromirror devices," Proc. SPIE 3221, pp. 6-11, 2000

[32] Q.S. Hanley, P.J. Verveer, M.J. Gemkow, D. Arndt-Jovin, T.M. Jovin, "An optical sectioning programmable array microscope implemented with a digital micromirror device," Journal of Microscopy, Vol. 196, Pt. 3 (1999), pp. 317-331
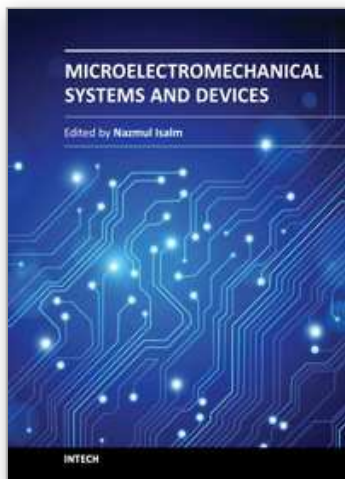
[33] E.P. Wagner II, B.W. Smith, S. Madden, J.D. Winefordner, M. Mignardi, "Construction and Evaluation of a Visible Spectrometer Using Digital Micromirror Spatial Light Modulation", Applied Spectroscopy, 49, 1715 (1995)

[34] D.M. Bloom, "The Grating Light Valve: revolutionizing display technology," Proc. International Society for Optical Engineering (SPIE), vol. 3013, Projection Displays III, pp. 165-71, 1997

[35] H. Urey, Retinal Scanning Displays, in Encyclopedia of Optical Engineering, to be published by Marcel-Dekker, 2003

[36] M. Freeman, "Miniature high-fidelity displays using a biaxial MEMS scanning mirror", MOEMS Display and Imaging Systems, Proc. SPIE Vol. 4985, San Jose, CA, Jan. 2003.

[37] H. Urey, "Torsional MEMS scanner design for high-resolution display systems," Proc. International Society for Optical Engineering (SPIE), vol. 4773, Optical Scanning II, pp. 27-37, 2002.

[38] Yan, S. Luanava, F.A. Dewitt IV, V. Cassanta, H. Urey, "Magnetic actuation for MEMS scanners for retinal scanning displays", Photonics West 2003, SPIE vol. 4985, pp.106-114, 2003

[39] Davis, W.O., Sprague, R., Miller, J., "MEMS-based pico projector display", Optical MEMs and Nanophotonics, 2008 IEEE/LEOS Internationall Conference on, Issue Date: 11-14 Aug. 2008, pp. 31 - 32

[40] Minsky, M. Microscopy Apparatus. US Patent # 3013467. 1957

[41] D.L. Dickensheets and G. S. Kino, "Silicon-micromachined scanning confocal optical microscope," Journal of Microelectromechanical Systems, Vol. 7, No. 1, pp. 38-47, March 1998.

[42] K. Murakami, A. Murata, T. Suga, H. Kitagawa, Y. Kamiya, M. Kubo, K. Matsumoto, H. Miyajima, and M. Katashiro, "A MINIATURE CONFOCAL OPTICAL MICROSCOPE WITH MEMS GIMBAL SCANNER", The 12th International Conference on Solid State Sensors, Actuators and Microsystems, Boston, June 8-12, 2003, pp. 587-590

[43] K.Murakami,et.al., "A MEMS gimbal scanner for a miniature confocal microscope", Optical-MEMS2002, 2002, TuA2 pp.9-10

[44] T. D. Wang, M. J. Mandella, C. H. Contag, and G. S. Kino, "Dual-axis confocal microscope for high-resolution in vivo imaging," Opt. Lett., 28(6), 414-416 (2003).

[45] J. T. C. Liu, M. J. Mandella, H. Ra, L. K. Wong, O. Solgaard, G. S. Kino, W. Piyawattanametha, C. H. Contag, and T. D. Wang, "Miniature near-infrared dual-axes confocal microscope utilizing a two-dimensional microelectromechanical systems scanner," Opt. Lett., 32(3), 256-258 (2007).

[46] H. Ra, W. Piyawattanametha, Y. Taguchi, D. Lee, M. J. Mandella, O. Solgaard, "Two-Dimensional MEMS Scanner for Dual-Axes Confocal Microscopy",Journal of Microelectromechanical Systems 16 (4), pp. 969-976 (2007).

[47] H. Ra, W. Piyawattanametha, M. J. Mandella, P.-L. Hsiung, J. Hardy, T. D. Wang, C. H. Contag, G. S. Kino, and O. Solgaard, "Three-dimensional in vivo imaging by a handheld dual-axes confocal microscope," Opt. Express, 16(10), 7224-7232 (2008).

[48] W. Piyawattanametha, H. Ra, M. J. Mandella, K. Loewke, T. D. Wang, G. S. Kino, O. Solgaard, and C. H. Contag, "3-d near-infrared fluorescence imaging using an mems-based miniature dual-axis confocal microscope," IEEE J. Sel. Top. Quantum Electron., 15(5), 1344-1350 (2009).

[49] Wibool Piyawattanametha, Hyejun Ra, Zhen Qiu, Shai Friedland, Jonathan T. C. Liu, Kevin Loewke, Gordon S. Kino, Olav Solgaard, Thomas D. Wang, Michael J. Mandella, and Christopher H. Contag, "In Vivo Near-infrared Confocal Microendoscopy in the Human Colorectal Tract", to be published in JBO 2012

[50] E.A. Swanson, D. Huang, M. R. Hee, J.G. Fujimoto, C.P. Lin, and C.A. Puliafito, "High-speed optical coherence domain reflectometry," Optics Letters, Vol. 17, Issue 2, pp 151, Jan. 1992

[51] D. Huang, E.A. Swanson, C.P. Lin, J.S. Schuman, W.G. Chang, M.R. Hee, T. Flotte, K. Gregory, C.A. Puliafito, and J.G. Fujimoto, "Optical Coherence Tomography", Science, 254:1178-1181, 1991

[52] Tearney, G.J., M.E. Brezinski, B.E. Bouma, S.A. Boppart, C. Pitvis, J.F. Southern, and J.G. Fujimoto, In vivo endoscopic optical biopsy with optical coherence tomography. Science, 1997. 276(5321): pp. 2037-9.

[53] A. M. Rollins, R. Ung-arunyawee, A. Chak, R. C. K. Wong, K. Kobayashi, M. V. Sivak, Jr., and J. A. Izatt, Opt. Lett. 24, 1358 (1999).

[54] Tuqiang Xie, Huikai Xie, Gary K. Fedder, and Yingtian Pan, "Endoscopic optical coherence tomography with a modified microelectromechanical systems mirror for detection of bladder cancers," APPLIED OPTICS, Vol. 42, No. 31, pp. 6422-6426, 1 November 2003.

[55] J. M. Zara, S. Yazdanfar, K. D. Rao, J. A. Izatt, and S. W. Smith, "Electrostatic micromachine scanning mirror for optical coherence tomography", OPTICS LETTERS, Vol. 28, No. 8, April 15, 2003, pp. 628-630

[56] A. D. Aguirre, P. R. Herz, Y. Chen, J. G. Fujimoto, W. Piyawattanametha, L. Fan, M. C. Wu, "Two-axis MEMS scanning catheter for ultrahigh resolution three-dimensional and en face imaging," Optics Express, Vol. 15, No. 5, pp. 2445-2453, March 2007.

[57] W. Piyawattanametha, P. Patterson, D. Hah, H. Toshiyoshi, and M. Wu, "A 2D Scanner by Surface and Bulk Micromachined Angular Vertical Comb Actuators," International Conference on Optical MEMS, August 18-21, Hawaii, USA, pp. 93-94

[58] W. Piyawattanametha, P. R. Patterson, D. Hah, H. Toshiyoshi, and M. C. Wu, "Surface- and Bulk- Micromachined Two-Dimensional Scanner Driven by Angular Vertical Comb Actuators," Journal of Microelectromechanical Systems, Vol. 14, No. 6, pp. 1329-1338, Dec. 2005.

[59] T. D. Kudrle, C. C. Wang, M. G. Bancu, J. C. Hsiao, A. Pareek, M. Waelti, G. A. Kirkos, T. Shone, C. D. Fung, and C. H. Mastrangelo, "Electrostatic Micromirror Arrays Fabricated with Bulk and Surface Micromachining Techniques," MEMS 2003, Kyoto, Japan, Jan. 2003, pp. 267-270

[60] R. K. Tyson and B. W. Frazier, "Microelectromechanical system programmable aberration generator for adaptive optics," Applied Optics Vol. 38 No. 1, pp 168-178, 1999

[61] C. Paterson, I. Munro, and J.C. Dainty, "A low cost adaptive optics system using a membrane mirror," Optics Express Vol. 6 No. 9 pp 175-185, 2000

[62] O. Albert, et al., "Smart microscope: an adaptive optics system using a membrane mirror," Optics Express Vol. 6 No. 9, pp 175-185, 2000

[63] G. Vdovin and V. Kiyko, "Intracavity control of a 200-W continuous-wave Nd:YAG laser by a micromachined deformable mirror," Optics Express Vol. 26 No. 11, pp. 798-800, 2001

[64] H. M. Dyson, R. M. Sharples, N. A. Dipper, G. V. Vdovin, " Cryogenic wavefront correction using membrane deformable mirrors, " Optics Express Vol. 8 No. 1, pp. 17-26, 2001

[65] L. Zhu et al., "Wave-front generation of Zernike polynomial modes with a micromachined membrane deformable mirror, " Applied Optics Vol. 38 No. 28, pp. 6019-6026, 1999

[66] Julie A. Perreault and Thomas G. Bifano, "HIGH-RESOLUTION WAVEFRONT CONTROL USING MICROMIRROR ARRAYS," The proceedings of Solid-State Sensor, Actuator and Microsystems Workshop Hilton Head Island, South Carolina, June 6-10, 2004, pp. 83-86

[67] Krishnamoorthy, R., Bifano, T. G., Vandelli, N., and Horenstein, M., "Development of MEMS deformable mirrors for phase modulation of light," Optical Engineering [36], pp. 542-548, 1997

[68] Currently MEMSCAP, Inc. Durham, NC

[69] Y. Hishinuma and E. H. Yang ,"Piezoelectric Unimorph Microactuator Arrays for Single-Crystal Silicon Continuous-Membrane Deformable Mirror" , JOURNAL OF MICROELECTROMECHANICAL SYSTEMS, VOL. 15, NO. 2, pp. 370-379, APRIL 2006.

[70] Michael A. Helmbrecht, Min He, Carl J. Kempf, Marc Besse, "MEMS DM development at Iris AO, Inc. ", Proc. SPIE 7931, 793108 (2011)

[71] M. Fujino, P. R. Patterson, H. Nguyen, W. Piyawattanametha, and M. C. Wu, "Monolithically Cascaded Micromirror Pair Driven by Angular Vertical Combs for Two-Axis Scanning," IEEE JOURNAL OF SELECTED TOPICS IN QUANTUM ELECTRONICS, VOL. 10, NO. 3, pp. 492-497, MAY/JUNE 2004

[72] H. Toshiyoshi and H. Fujita, "Electrostataic Micro Torsion Mirrors for an Optical Switch Matrix," IEEE J. Microelectromechanical Systems, Vol. 5, p. 231, 1996.

[73] L.Y. Lin, E.L. Goldstein, and R.W. Tkach, "Free-space micromachined optical switches with submillisecond switching time for large-scale optical crossconnects," IEEE Photonics Technology Letters, vol.10, p.525-7, 1998.

[74] B. Hehin, K.Y. Lau, and R.S. Muller, "Magnetically actuated micromirrors for fiber-optic switching," Solid-State Sensors and Actuator Workshop, Hilton Head Island, South Carolina, 1998.

[75] R. L. Wood, R. Mahadevan, and E. Hill, "MEMS 2-D matrix switch," 2002 Optical Fiber Communication (OFC) Conference, Paper TuO2, Anaheim California, 2002.

[76] Y. Yoon, K. Bae, and H. Choi, "An optical switch with newly designed electrostatic actuators for optical cross connects," 2002 IEEE/LEOS International Conference on Optical MEMS, Lugano, Switzerland, 2002.

[77] L.Y. Lin, E.L. Goldstein, and R.W. Tkach, "Angular-precision enhancement in free-space micromachined optical switches," IEEE Photonics Technology Letters, vol.11, p.1253-5, 1999.

[78] L.Y. Lin, E.L. Goldstein, and R.W. Tkach, "Free-space micromachined optical switches for optical networking," IEEE Journal of Selected Topics in Quantum Electronics, Vol. 5, P.4-9, 1999.

[79] T. Akiyama and H. Fujita, "A quantitative analysis of scratch drive actuator using buckling motion", Proc. 8th IEEE International MEMS Workshop, pp. 310 - 315, 1995.

[80] L.-Y. Lin, E.L. Goldstein, R.W. Tkach, "On the expandability of free-space micromachined optical cross connects," J. Lightwave Technology, Vol. 18, pp. 482 – 489, 2000.

[81] Li Fan, S. Gloeckner, P. D. Dobblelaere, S. Patra, D. Reiley, C. King, T. Yeh, J. Gritters, S. Gutierrez, Y. Loke, M. Harburn, R. Chen, E. Kruglick, M. Wu and A. Husain, "Digital MEMS switch for planar photonic crossconnects," 2002 Optical Fiber Communication (OFC) Conference, Paper TuO4, Anaheim, California, 2002

[82] R.T. Chen, H. Nguyen, M.C. Wu, "A high-speed low-voltage stress-induced micromachined 2x2 optical switch," IEEE Photonics Technol. Lett., Vol. 11, pp.1396-8, November 1999.

[83] Marxer, C.; de Rooij, N.F. "Micro-opto-mechanical 2x2 switch for single-mode fibers based on plasma-etched silicon mirror and electrostatic actuation," J. Lightwave Technology, vol. 17, no. 1, pp. 2-6, Jan. 1999.

[84] Noell, W.; Clerc, P.-A.; Dellmann, L.; Guldimann, B.; Herzig, H.-P.; Manzardo, O.; Marxer, C.R.; Weible, K.J.; Dandliker, R.; de Rooij, N. "Applications of SOI-based optical MEMS," IEEE J. Selected Topics in Quantum Electronics, vol. 8, no. 1, pp. 148-154, 2002.

[85] Marxer, C.; Thio, C.; Gretillat, M.-A.; de Rooij, N.F.; Battig, R.; Anthamatten, O.; Valk, B.; Vogel, P. "Vertical mirrors fabricated by deep reactive ion etching for fiber-optic switching applications," J. Microelectromechanical Systems, vol. 6, no. 3, pp.277-85, Sept. 1997.

[86] Neilson, D.T., et al.,"Fully Provisioned 112x112 Micro-Mechanical Optical Crossconnect With 35.8Tb/s Demonstrated Capacity," Optical Fiber Communication Conference, OFC 2000, March 7-10, Baltimore, MD, Vol. 4, pp.202-204.

[87] Lin, L.Y., Goldstein, E.L., "Opportunities and Challenges for MEMS in Lightwave Communications," IEEE J. Sel. Topics Quantum Elec., Vol. 8, No. 1, p.163, 2002.

[88] Syms, R.R.A., "Scaling Laws for MEMS Mirror-Rotation Optical Cross Connect Switches," IEEE J. Lightwave Tech., Vol. 20, No. 7, p. 1084, 2002.

[89] J. Kim et al., "1100x1100 port MEMS-based optical crossconnect with 4-db maximum loss," IEEE Photonics Technol. Lett., Vol. 15, pp.1537-9, November 2003.

[90] D. T. Neilson and R. Ryf, "Scalable micro mechanical optical crossconnects," 2000 IEEE/LEOS Annual Meeting, Paper ME2.

[91] V. A. Aksyuk et al., "238x238 micromechanical optical cross connect," IEEE Photonics Technol. Lett., Vol. 15, pp.587-9, April 2003.

[92] V. A. Aksyuk et al., "Beam-steering micromirrors for large optical cross-connects," IEEE J. Lightwave Tech., Vol. 21, No. 3, p. 634, 2003.

[93] M. Kozhevnikov et al., "Micromechanical optical crossconnect with 4-F relay imaging optics," IEEE Photonics Technol. Lett., Vol. 16, pp.275-7, Jan. 2004.

[94] R. Ryf et al., "1296-port MEMS transparent optical crossconnect with 2.07Petabit/s switch capacity," in Proceedings of 2001 OFC postdeadline paper, PD28.

[95] N. Yazdi, H. Sane, T. D. Kudrle, and C. H. Mastrangelo, "Robust sliding-mode control of electrostatic torsional micromirrors beyond the pull-in limit," 12th International Conference on Solid-State Sensors, Actuators and Microsystems (TRANSDUCERS 2003, 8-12 June 2003), vol. 2, pp.1450 – 1453.

[96] T. D. Kudrle, G. M. Shedd, C. C. Wang, J. C. Hsiao, M. G. Bancu, G. A. Kirkos, N. Yazdi, M. Waelti, H. Sane, and C. H. Mastrangelo, "Pull-in suppression and torque magnification in parallel plate electrostatic actuators with side electrodes," 12th

International Conference on Solid-State Sensors, Actuators and Microsystems (TRANSDUCERS 2003, 8-12 June 2003), vol. 1, pp.360 – 363.

[97] T. D. Kudrle, C. C. Wang, M. G. Bancu, J. C. Hsiao, A. Pareek, M. Waelti, G. A. Kirkos, T. Shone, C. D. Fung, and C. H. Mastrangelo, "Electrostatic micromirror arrays fabricated with bulk and surface micromachining techniques," IEEE The Sixteenth Annual International Conference on Micro Electro Mechanical Systems (MEMS 2003, 19-23 Jan. 2003), pp.267 – 270.

[98] Sawada, R.; Yamaguchi, J.; Higurashi, E.; Shimizu, A.; Yamamoto, T.; Takeuchi, N.; Uenishi, Y. "Single Si crystal 1024ch MEMS mirror based on terraced electrodes and a high-aspect ratio torsion spring for 3-D cross-connect switch," 2002 IEEE/LEOS International Conference on Optical MEMs, pp. 11 –12, 2002.

[99] Sawada, R.; Yamaguchi, J.; Higurashi, E.; Shimizu, A.; Yamamoto, T.; Takeuchi, N.; Uenishi, Y. "Improved single crystalline mirror actuated electrostatically by terraced electrodes with high aspect-ratio torsion spring," 2003 IEEE/LEOS International Conference on Optical MEMs, pp. 153 –154, 2003.

[100] Y. Mizuno et al., "A 2-axis comb-driven micromirror array for 3D MEMS switches," 2002 IEEE/LEOS International Conference on Optical MEMs, pp. 17 –18, 2002.

[101] N. Kouma et al., "A multi-step DRIE process for a 128x128 micromirror array," 2003 IEEE/LEOS International Conference on Optical MEMs, pp. 53 –54, 2003.

[102] P. B. Chu et al., "Design and Nonlinear Servo Control of MEMS Mirrors and Their Performance in a Large Port-Count Optical Switch," Journal of Microelectromechanical Systems, VOL. 14, NO. 2, pp. 261-273, APRIL 2005.

[103] J. I. Dadap et al., "Modular MEMS-based optical cross-connect with large port-count," IEEE Photonics Technol. Lett., Vol. 15, pp.1773-5, Dec. 2003.

[104] C. Pu et al., "Electrostatic Actuation of Three-Dimensional MEMS Mirrors Using Sidewall Electrodes, IEEE Journal of Selected Topics in Quantum Electronics," VOL. 10, NO. 3, pp. 472-477, MAY/JUNE 2004.

[105] X. Zheng et al., "Three-dimensional MEMS photonic cross-connect switch design and performance," IEEE J. Sel. Topics Quantum Elec., Vol. 9, No. 2, p.571, 2003.

[106] Aksyuk, V.A., Pardo, F., Bolle, C.A., Arney, S., Giles, C.R., Bishop, D.J., "Lucent Microstar micromirror array technology for large optical crossconnects," Proceedings of the SPIE, MOEMS and Miniaturized Systems, Sept. 2000, Santa Clara, CA, pp. 320-324.

[107] Aksyuk V.A., Simon, M.E., Pardo, F., Arney S., Lopez, D., and Villanueva, A., "Optical MEMS Design for Telecommunications Applications," 2002 Solid-State Sensor and Actuator Workshop Tech. Digest, June 2-6, Hilton Head, SC, pp.1-6.

[108] A. Gasparyan, et al., "Drift-free, 1000G mechanical shock tolerant single-crystal silicon two-axis MEMS tilting mirrors in a 1000x1000-port optical crossconnect", in Proceedings of 2003 OFC postdeadline paper, PD36.

[109] V.A. Aksyuk et al., "238×238 surface micromachined optical crossconnect with 2dB maximum loss," OFC (Optical Fiber Communication) 2002, Postdeadline paper, FB9-1 – FB 9-3.

Microelectromechanical Systems and Devices

Edited by Dr Nazmul Islam

ISBN 978-953-51-0306-6

Hard cover, 480 pages

Publisher InTech

Published online 28, March, 2012

Published in print edition March, 2012

The advances of microelectromechanical systems (MEMS) and devices have been instrumental in the demonstration of new devices and applications, and even in the creation of new fields of research and development: bioMEMS, actuators, microfluidic devices, RF and optical MEMS. Experience indicates a need for MEMS book covering these materials as well as the most important process steps in bulk micro-machining and modeling. We are very pleased to present this book that contains 18 chapters, written by the experts in the field of MEMS. These chapters are groups into four broad sections of BioMEMS Devices, MEMS characterization and micromachining, RF and Optical MEMS, and MEMS based Actuators. The book starts with the emerging field of bioMEMS, including MEMS coil for retinal prostheses, DNA extraction by micro/bio-fluidics devices and acoustic biosensors. MEMS characterization, micromachining, macromodels, RF and Optical MEMS switches are discussed in next sections. The book concludes with the emphasis on MEMS based actuators.

INTECH

open science | open minds